ISSN 0280-5316
ISRN LUTFD2/TFRT--5746--SE

Vehicle Dynamics Control for Rollover Mitigation

Ola Palm

Department of Automatic Control
Lund Institute of Technology
May 2005

Department of Automatic Control
Lund Institute of Technology
Box 118
SE-221 00 Lund Sweden

Document name
MASTER THESIS

Date of issue
May 2005

Document Number
ISRNLUTFD2/TFRT--5746--SE

Author(s)
Ola Palm

Supervisor
Jens Kalkkuhl at DaimlerChrysler in Germany
Tore Hägglund at Automatic Control in Lund

Sponsoring organization

Title and subtitle
Vehicle Dynamics Control for Rollover Mitigation (Fordonsdynamikreglering för vältskydd)

Abstract
Characterized by a high ratio between the height of center of gravity and the track-width, commercial vehicle dynamics differ from passenger car dynamics. The roll stability limit, measured in terms of lateral acceleration, is much lower, while longitudinal and lateral load transfer during braking and cornering reduce the yaw stability, resulting in roll motion. Rollovers are dangerous and possible lethal accidents. This master's thesis proposes how to detect and prevent untripped rollovers on commercial vans.

Two methods to predict and detect rollover are examined. An analytical one, which uses the spring deflection sensors to measure the load distribution and therefore detects wheel liftoff as an indication of possible rollover. The other one, which is used in the developed controller, considers the potential and kinetic roll energy of the vehicle.

A new control system is introduced to stabilize the roll and slip dynamics of the vehicle. It is based on an energy-related Lyapunov function, which controls the yaw rate to accomplish the objectives. The controller outputs the desired braking forces on each wheel that will stabilize the vehicle. Finally, differential braking is used to take out energy from the system.

Simulations of extreme maneuvers show that the control system prevents the vehicle from rollover and skidding. They also indicate that the controller is robust against uncertainties in the load conditions. Comparisons with an existing LQ-controller confirm further the promising results of the Lyapunov controller.

Keywords
Rollover prevention and detection, skidding, vehicle dynamics, stability, nonlinear, control, mitigation, Lyapunov

Classification system and/or index terms (if any)

Supplementary bibliographical information

ISSN and key title
0280-5316

ISBN

Language
English

Number of pages
76

Recipient's notes

Security classification

Acknowledgement

The research was accomplished between October 2004 and March 2005 at the Vehicle Systems Dynamics, DaimlerChrysler R&T, outside Stuttgart, Germany. It guided the way to this thesis report at the department of Automatic Control, Lund Institute of Technology.

First of all I would like to thank my supervisors, Doctor Jens Kalkkuhl at DaimlerChrysler R&T, Vehicle Systems Dynamics, and Professor Tore Hägglund at Lund Institute of Technology, department of Automatic Control, for excellent supervision and guidance.

I also want to express my gratitude to Doctor Tran and all the students related to the Vehicle Systems Dynamics department at DaimlerChrysler R&T.

Finally, thanks everyone for proof-reading the report and providing me with valuable comments.

Lund, May 22 2005

Ola Palm

Notation

Symbols

x	italic letters are used in mathematical text
$\boldsymbol{x}, \tilde{\boldsymbol{\omega}}$	boldface letters are used for vectors and tensors
$\vec{\boldsymbol{v}}$	boldface letters with arrows are used for geometrical represented vectors
$\boldsymbol{C}$	capital and boldface letters are used for matrices
E	capital letters are used for sets
$\Re$	the set of real numbers
V	Lyapunov function
$u, \boldsymbol{u}$	control input
$\boldsymbol{x}$	state vector
t	time

Subscripts

$_F$	front wheel
$_R$	rear wheel
$_i$	wheel number; i=1 (front left), 2 (front right), 3 (rear left), 4 (rear right)
$_x$	in the x-direction of the coordinate system
$_y$	in the y-direction of the coordinate system
$_z$	in the z-direction of the coordinate system
$_w$	wheel parameter
$_{max}$	maximum value
$_{CoG}$	center of gravity
$_{des}$	desired value
$_{crit}$	critical value

Operators and Functions

$\|\boldsymbol{x}\|$	Euclidian norm of $\boldsymbol{x}$
$\dot{V} = \frac{dV}{dt}$	time derivative of V
$\frac{\partial V}{\partial x}$	partial derivative of V with respect to x
$\frac{\partial V}{\partial \boldsymbol{x}} = \left(\frac{\partial V}{\partial x_1}, ..., \frac{\partial V}{\partial x_n}\right)^{\mathrm{T}}$	gradient of V

Abbreviations

ABS	Anti-lock Brake System
ESP	Electronic Stability Program
clf	control Lyapunov function
CoG	Center of Gravity
CASCaDE	Computer Aided Simulation of Car, Driver, and Environment

Vehicle Nomenclature

Symbol	**Definition**	**Unit**
v_x	longitudinal velocity	m/s
v_y	lateral velocity	m/s
φ	roll angle	rad, $^\circ$
$\dot{\varphi}$	roll rate	rad/s
$\dot{\psi}$	yaw rate	rad/s
a_x	longitudinal acceleration	m/s^2
a_y	lateral acceleration	m/s^2
$F_{x,i}$	longitudinal force at wheel i	N
$F_{y,i}$	lateral force at wheel i	N
$F_{z,i}$	normal force at wheel i	N
$M_{z,i}$	angular momentum at wheel i	Nm
δ_i	steering angle of wheel i	rad, $^\circ$
ω_w	wheel rotation speed	rad/s
μ	road-tire coefficient of friction	unitless
m	mass	kg
J_{xx}	moment of inertia about the x-axis	kgm^2
J_{yy}	moment of inertia about the y-axis	kgm^2
J_{zz}	moment of inertia about the z-axis	kgm^2
l_F	horizontal distance from the front axle to the CoG	m
l_R	horizontal distance from the rear axle to the CoG	m
h_{CoG}	height from the ground to the CoG	m
s_F	front track width	m
s_R	rear track width	m
s	mean track width	m
c_φ	roll stiffness, mean of both axles	Nm/rad
d_φ	roll damping, mean of both axles	Nm/rad

Other used variables are defined in the report.

Contents

List of Figures

List of Tables

Chapter 1

Introduction

This chapter introduces some basic background facts about rollover and the origin of this master's thesis work. It also discusses the purpose and objectives, how the work has been structured, used software, and some assumptions. Finally, this report is outlined.

1.1 Background

Rollover occurs when a vehicle flips over on the side. It is possible to distinguish between two types of rollover; tripped and untripped. Tripped rollover occurs when the vehicle has started to skid, then gets grip due to higher friction or hits an obstacle, and finally rolls over. Untripped rollover is caused by the driver, either on purpose during extreme maneuvers, or in panic situations, [6].

Every year more than 40,000 people are killed in car accidents in Europe and over 1.7 million people are injured, [2]. Rollover is one of the most dangerous car crashes on European highways, responsible for many of the killed people. Vehicles with a high center of gravity, e.g. vans, commercial vehicles, and Sport Utility Vehicles (SUVs), are becoming more popular. Since the ratio between the height of the center of gravity and the track width is bigger for these vehicles than normal passenger cars, they are more likely to rollover during extreme maneuvers, [3].

The tripped rollover is well understood, and the most common type. It can be avoided if a control system prevents the vehicle from skidding, e.g.

the ESP[1] system. The untripped rollover is not so well understood, but it can be avoided if a control system lets the vehicle deviate from the desired driving path, [6].

To be able to increase the safety on the European roads and to decrease the number of killed and injured, the CEmACS[2] project is a part of EU's sixth framework . The project's main goal is to improve the driver and passenger safety by accident avoidance and accident mitigation. This is done through development of active systems that will respond faster and more reliable in emergency situations than the average driver. Four European universities, Lund Institute of Technology among them, and DaimlerChrysler are parts of the project. This thesis work, "Vehicle Dynamics Control for Rollover Mitigation", is one part of the traffic safety work in the European CEmACS programme, see [2].

1.2 Purpose and Objectives

The main purpose of this thesis is to design, implement, and simulate a control system (related to energy), which prevents a commercial van from rollover. The objectives of the thesis can be organized in the following way;

- prevent untripped rollovers
- minimize the side slip
- minimize the deviation from the desired driving path
- adopt for changes in load parameters.

From the results reached in this report, DaimlerChrysler can decide whether the design of this controller is of interest to prevent rollover of vehicles with a relatively high center of gravity.

1.3 Method

All work has been done at DaimlerChrysler R&T, Vehicle Systems Dynamics, in Esslingen outside Stuttgart, Germany. The work has been separated

[1] Electronic Stability Program
[2] Complex Embedded Automotive Control Systems

into seven parts;

- study control theory and the underlying dynamics of vehicles and tires
- derive a vehicle model with roll dynamics
- find a way to detect rollover
- design a controller to accomplish the objectives
- implement the controller in Matlab
- simulate the vehicle in Simulink for different maneuvers, velocities, and load conditions, then analyze the results
- do a robustness analysis of the controller and adopt for changes in parameters.

1.3.1 Software

Matlab [10] is the main software used for computation, model implementation, and simulation. The Matlab simulation tool Simulink [10], which is used for modeling and simulating dynamic systems, has been playing a major role during this work. Together with a CASCaDE[3]-model of the vehicle, it has been used for modeling and simulating the commercial van. This text was produced with LaTeX [13].

1.4 Limitations and Assumptions

To be able to work properly, the controller needs to know the states of the vehicle. Usually this is accomplished by using an observer, but since that is outside the scope of this thesis it is assumed that all states are measurable.

The load conditions of the vehicle are unknown, i.e. the mass, the position of the center of gravity, and the moments of inertia are not known.

The only actuators are the controlled brakes. Therefore, the only way to mitigate rollover is to brake independently on the different wheels.

[3]Computer Aided Simulation of Car, Driver, and Environment

1.5 Outline of the Thesis

This thesis is outlined as follows.

Chapter 2: Presents general nonlinear theory and Lyapunov theory. It gives the theoretical background needed to understand the controller design.

Chapter 3: This chapter describes some basic facts about vehicle dynamics and brings up different models. First the tires are discussed, then a model of the rolling chassis is derived, and finally everything is combined in the vehicle model.

Chapter 4: Here the rollover detection is examined. Different approaches to detect and predict rollover, both theoretical and analytical, are discussed.

Chapter 5: This chapter introduces the rollover mitigation controller. The control strategy is explained and the control laws are derived. Finally the performance of the controller is demonstrated through simulations and discussions of different maneuvers, velocities, and load conditions. The controller is also compared to an already existing LQ-controller and to a vehicle without any roll control at all.

Chapter 6: This chapter concludes the thesis by summing up the main results and discussions from rollover detection and mitigation.

Chapter 7: The last chapter states some proposals for future work.

Chapter 2

System and Control Theory

This chapter first presents some nonlinear theory for general systems, see [16]. Then the control theory used in this thesis work is presented, including important definitions and theorems.

2.1 General Nonlinear Theory

A nonlinear dynamic system can usually be represented by a set of nonlinear differential equations in the form

$$\dot{\boldsymbol{x}} = \boldsymbol{f}(\boldsymbol{x}, t) \tag{2.1}$$

where $\boldsymbol{x}$ is a $n \times 1$ state vector and $\boldsymbol{f}$ is a $n \times 1$ nonlinear vector function. A point is a particular value of the state vector because the value corresponds to a point in the state-space. The number of states n is called the order of the system. A solution $\boldsymbol{x}(t)$ of the equations (2.1) corresponds to a curve in state space as t varies from zero to infinity; this curve is called a state or system trajectory.

Note that although equation (2.1) does not explicitly contain any control input $\boldsymbol{u}$ as a variable, it is directly applicable to feedback control systems. That is because equation (2.1) can describe the closed-loop dynamics of a feedback control system, where the control input $\boldsymbol{u}$ is a function of the states $\boldsymbol{x}$ and the time t; therefore disappearing in the closed-loop dynamics. If the plant dynamics is

$$\dot{\boldsymbol{x}} = \boldsymbol{f}(\boldsymbol{x}, \boldsymbol{u}, t) \tag{2.2}$$

and the control input has been derived to be

$$\boldsymbol{u} = \boldsymbol{g}(\boldsymbol{x}, t) \tag{2.3}$$

then the closed-loop dynamics is

$$\dot{\boldsymbol{x}} = \boldsymbol{f}\big(\boldsymbol{x}, \boldsymbol{g}(\boldsymbol{x}, t), t\big) \tag{2.4}$$

This can be rewritten in the form (2.1). Equation (2.1) can of course also represent dynamic systems where no control signals are present.

A special class of nonlinear systems are linear systems. They are on the form

$$\dot{\boldsymbol{x}} = \boldsymbol{A}(t)\boldsymbol{x} \tag{2.5}$$

where $\boldsymbol{A}(t)$ is a $n \times n$ matrix.

Linear systems are either time-varying or time-invariant, depending on whether the system matrix $\boldsymbol{A}$ varies with time or not. In the more general theory of nonlinear systems, these adjectives are replaced in the following definition.

Definition 2.1 *The nonlinear system (2.1) is said to be autonomous if $\boldsymbol{f}$ does not depend explicitly on time t, i.e., if the system can be written*

$$\dot{\boldsymbol{x}} = \boldsymbol{f}(\boldsymbol{x}) \tag{2.6}$$

Otherwise the system is called non-autonomous.

Note that for control systems, the above definition is made on the closed-loop dynamics. From now on all the discussed systems in this thesis will be autonomous.

2.1.1 Equilibrium Points

It is possible for a system trajectory to correspond to only a single point, which is called an equilibrium point.

Definition 2.2 *A state $\boldsymbol{x}_e$ is an equilibrium state (or point) of the system if once $\boldsymbol{x}(t)$ is equal to $\boldsymbol{x}_e$, it remains equal to $\boldsymbol{x}_e$ for all future time.*

This means that the constant vector $\boldsymbol{x}_e$ satisfies

$$\mathbf{0} = \boldsymbol{f}(\boldsymbol{x}_e) \tag{2.7}$$

Equilibrium points can be found by solving these nonlinear algebraic equations (2.7). A nonlinear system can have none, several, or infinitely many equilibrium points.

A linear time-invariant system

$$\dot{\boldsymbol{x}} = \boldsymbol{A}\boldsymbol{x} \tag{2.8}$$

has the origin $\mathbf{0}$ as a single equilibrium point if $\boldsymbol{A}$ is nonsingular. It has infinitely many equilibrium points contained in the null-space of the matrix $\boldsymbol{A}$, i.e. in the subspace defined by $\boldsymbol{A}\boldsymbol{x} = \mathbf{0}$, if $\boldsymbol{A}$ is singular.

Different stability concepts of nonlinear systems are properties not of the dynamic system as a whole, but rather of its individual solutions. The following definition defines the stability class of a certain equilibrium point.

Definition 2.3 *Given the system (2.6), assume that $\boldsymbol{x}_e$ is an equilibrium point and $\boldsymbol{x}(0)$ represents the initial state. Then the equilibrium point $\boldsymbol{x}_e$ is said to be*

- *stable, if for any $\varepsilon > 0$ there exists some $\delta(\varepsilon) > 0$ such that*

$$\|\boldsymbol{x}(0) - \boldsymbol{x}_e\| < \delta \Rightarrow \|\boldsymbol{x}(t) - \boldsymbol{x}_e\| < \varepsilon,\ \forall\, t \geq 0 \tag{2.9}$$

- *unstable, if not stable*

- *asymptotically stable, if it is stable and if there exists some $\delta > 0$ such that*

$$\|\boldsymbol{x}(0) - \boldsymbol{x}_e\| < \delta \Rightarrow \boldsymbol{x}(t) \rightarrow \boldsymbol{x}_e \text{ as } t \rightarrow \infty \tag{2.10}$$

- *exponentially stable, if there exist two constants $\alpha > 0$ and $\lambda > 0$ such that*

$$\|\boldsymbol{x}(t) - \boldsymbol{x}_e\| \leq \alpha \|\boldsymbol{x}(0) - \boldsymbol{x}_e\| e^{-\lambda t},\ \forall\, t > 0 \tag{2.11}$$

  in some ball $\|\boldsymbol{x}(0) - \boldsymbol{x}_e\| < \delta$, $\delta > 0$, around the equilibrium point

- *globally asymptotically (or exponentially) stable, if it is asymptotically (or exponentially) stable for any initial states.*

The stability definition above is often referred to as stability in the sense of Lyapunov. A stable equilibrium point means that the system trajectory can be kept arbitrarily close to this point by starting sufficiently close to it. An asymptotically stable equilibrium point is stable, and states started close to this point will converge to this point as time goes to infinity. An equilibrium point, which is stable but not asymptotically stable, is said to be marginally stable. The exponential stability (2.11) means that the states converges to the equilibrium point faster than an exponential function. The stability discussion above is characterizing the local behavior of systems, i.e., how the states develop after starting near the equilibrium point. Instead, global concepts tell how the system will behave when the initial states is some distance away from the equilibrium point. Therefore, a globally asymptotically stable equilibrium point means that all solutions, regardless of starting point, will converge to it. Clearly, this is in most cases a desirable property of a control system since it then can deal better with perturbations and disturbances.

2.2 Lyapunov Theory

To be able to show which type of stability a certain equilibrium point corresponds to, equation (2.6) must be solved to find $\boldsymbol{x}(t)$. In general, this is not possible to do analytically. Stability can however be proved using *Lyapunov's direct method*. This method determines the system's stability properties from the properties of $\boldsymbol{f}(\boldsymbol{x})$ and its relation to a so-called *Lyapunov function* $V(\boldsymbol{x})$. The general interpretation of the Lyapunov function is that it is a measurement of how far the system is from the equilibrium; when this measurement decreases the system moves towards the equilibrium point.

The procedure of Lyapunov's direct method is to generate a scalar "energy-like" Lyapunov function $V(\boldsymbol{x})$ for the dynamic system, and then examine the time variation of it. In this way, conclusions can be drawn on the stability of the set of differential equations without using the stability definitions (see page 7) above. The definitions, theorems, and facts below are collected from [4], [5], [9], [15], and [16].

Definition 2.4 *A function $V(\boldsymbol{x})$ is said to be*

- *positive definite if* $V(\mathbf{0}) = \mathbf{0}$ *and* $V(\boldsymbol{x}) > 0,\ \boldsymbol{x} \neq 0$

- *positive semi-definite if* $V(\mathbf{0}) = \mathbf{0}$ *and* $V(\boldsymbol{x}) \geq 0,\ \boldsymbol{x} \neq 0$
- *negative (semi-)definite if* $-V(\boldsymbol{x})$ *is positive (semi-)definite*
- *radially unbounded if* $V(\boldsymbol{x}) \to \infty$ *as* $\|\boldsymbol{x}\| \to \infty$.

The definition above can be locally or globally definite depending on where in the state space it is valid.

Theorem 2.1 (LaSalle-Yoshizawa) *Let* $\boldsymbol{x}_e = \mathbf{0}$ *be an equilibrium point of (2.6) and suppose* $\boldsymbol{f}$ *is locally Lipschitz in* $\boldsymbol{x}$ *uniformly in* t. *Let* $V(\boldsymbol{x})$ *be a scalar, continuously differentiable function of the states* $\boldsymbol{x}$ *such that*

- $V(\boldsymbol{x})$ *is positive definite*
- $V(\boldsymbol{x})$ *is radially unbounded*
- $\dot{V}(\boldsymbol{x}) = \dfrac{\partial V(\boldsymbol{x})}{\partial \boldsymbol{x}}\ \dot{\boldsymbol{x}} = \dfrac{\partial V(\boldsymbol{x})}{\partial \boldsymbol{x}} f(\boldsymbol{x}) \leq -W(\boldsymbol{x}),\ \forall\ t \geq 0,\ \forall\ \boldsymbol{x} \in \Re^n$, *where* $W(\boldsymbol{x})$ *is a continuous and positive semi-definite function.*

Then all solutions of (2.6) are globally bounded and satisfy $\lim_{t \to \infty} W(\boldsymbol{x}(t)) = 0$. *In addition, if* $W(\boldsymbol{x})$ *is positive definite, then the equilibrium* $\boldsymbol{x}_e = \mathbf{0}$ *is globally asymptotically stable (GAS).*

Proof: See [9]. □

When $\dot{V}(\boldsymbol{x})$ is only negative semi-definite the following theorem can be used to prove stability.

Theorem 2.2 *Let* $\boldsymbol{x}_e = \mathbf{0}$ *be the only equilibrium of (2.6). Let* $V(\boldsymbol{x})$ *be a scalar, continuously differentiable function of the states* $\boldsymbol{x}$ *such that*

- $V(\boldsymbol{x})$ *is positive definite*
- $V(\boldsymbol{x})$ *is radially unbounded*
- $\dot{V}(\boldsymbol{x})$ *is negative semi-definite.*

Let $E = \{\boldsymbol{x} \in \Re^n | \dot{V}(\boldsymbol{x}) = 0\}$, *and suppose that no solution other than* $\boldsymbol{x}(t) \equiv \mathbf{0}$ *can stay forever in* E. *Then the equilibrium* $\boldsymbol{x}_e = \mathbf{0}$ *is globally asymptotically stable (GAS).*

Proof: See [9]. □

The theorems above assume that the origin $\boldsymbol{x}_e = \mathbf{0}$ is the equilibrium point. Every other equilibrium point can be moved to the origin through defining a new set of states $\boldsymbol{x}_{new} = \boldsymbol{x} - \boldsymbol{x}_e$. This validates the theorems for every possible equilibrium point.

Lyapunov functions are very powerful tools when determining the stability properties of equilibrium points. No knowledge of the solution to the system of differential equations is needed. Many other tools to determine the stability are local theories, whereas the Lyapunov theory presents more global results. It is possible to estimate the extent of the basin of attraction of an equilibrium point. The basin of attraction is the domain such that all solutions starting within the domain approach the equilibrium point, see [4]. The theorem below explains how to decide this domain.

Theorem 2.3 (Basin of attraction) *Assume that for the system (2.6) there exist a number $d > 0$ and a function V that satisfies the conditions for Theorem 2.2 in the set*

$$M_d = \{\boldsymbol{x} \mid V(\boldsymbol{x}) < d\} \tag{2.12}$$

Then all solutions starting in the interior of M_d remains there. If, in addition, no other solutions but the equilibrium point $\boldsymbol{x}_e$ remain in the subset of M_d where $\dot{V}(\boldsymbol{x}) = 0$, then all solutions starting in the interior of M_d will converge to $\boldsymbol{x}_e$.

Proof: See [5]. □

A Geometrical Interpretation of Lyapunov's Direct Method can be found in [4].

2.3 Lyapunov Theory and Control Design

This section discusses how closed loop systems can be designed so that the Lyapunov criterions are fulfilled, which results in globally asymptotically stable equilibrium points.

Consider the system with an input $\boldsymbol{u}$

$$\dot{\boldsymbol{x}} = \boldsymbol{f}(\boldsymbol{x}, \boldsymbol{u}) \tag{2.13}$$

The goal is to find a control law $\boldsymbol{u} = \boldsymbol{g}(\boldsymbol{x})$, which makes some desired states of the closed loop system asymptotically stable. By using a Lya-

punov function $V(\boldsymbol{x})$ and choosing $\boldsymbol{g}(\boldsymbol{x})$ so that

$$\dot{V}(\boldsymbol{x}) = \frac{\partial V(\boldsymbol{x})}{\partial \boldsymbol{x}} f(\boldsymbol{x}, \boldsymbol{g}(\boldsymbol{x})) = -W(\boldsymbol{x}) \tag{2.14}$$

where $W(\boldsymbol{x})$ is positive definite, closed loop stability is given by Theorem 2.1. It can be difficult to know how to choose $V(\boldsymbol{x})$ and $W(\boldsymbol{x})$. The following definition makes it easier.

Definition 2.5 (Control Lyapunov Function) *A smooth, positive definite, radially unbounded, and scalar function $V(\boldsymbol{x})$ is called a control Lyapunov function for (2.13) if for all $\boldsymbol{x} \neq 0$*

$$\dot{V}(\boldsymbol{x}) = \frac{\partial V(\boldsymbol{x})}{\partial \boldsymbol{x}} f(\boldsymbol{x}, \boldsymbol{u}) < 0 \text{ for some } \boldsymbol{u}. \tag{2.15}$$

A system possesses a clf[1] if a good choice of $V(\boldsymbol{x})$ and $W(\boldsymbol{x})$ exists. Artstein, see [9], showed that (2.15) is not only necessary, but also sufficient for the existence of a control law satisfying (2.14), i.e., the existence of a clf is equivalent to global asymptotic stability.

[1] control Lyapunov function

Chapter 3

General Vehicle Dynamics

The used coordinate systems are in the DIN (Deutsches Institut für Normung) standard; x, y, z, right-hand orthogonal with the z-axis in local upward direction. The three-dimensional Cartesian vehicle-attached coordinate system has the x-direction in the direction where the car is moving, the y-direction out through the left side of the car, and the z-direction up through the roof of the car. The yaw rate and the roll angle of the vehicle are defined so that they are positive when the vehicle is cornering to the left, and vice versa.

3.1 Vehicle Dynamics and Tire Models

The forces, which the driver can influence, are induced by the tires. To be able to produce forces a tire needs to slip, which can take place in two directions, laterally and longitudinally. There exists two quantities to describe the two different slips, [14],

- the (tire) slip angle α characterizing the lateral slip
- the longitudinal slip λ.

The tire slip angle α is defined as the angle between the wheel velocity vector $\vec{v}_w$ and the x_w-axis

$$\tan(\alpha) = \frac{v_{y_w}}{v_{x_w}} \tag{3.1}$$

where v_{x_w} and v_{y_w} are the longitudinal and lateral velocities of the wheel in a coordinate system attached to the wheel, see Figure 3.1. The longitudinal slip is defined as

$$\lambda = \frac{r_{dyn}\omega_w - v_{x_w}}{\max(r_{dyn}\omega_w, v_{x_w})} \tag{3.2}$$

where

r_{dyn} = dynamic rolling radius

ω_w = wheel rotation speed

The longitudinal slip can assume values in the interval $\lambda = [-1, 1]$. A negative value indicates braking operation, while a positive value corresponds to acceleration.

Lateral slip occurs when the velocity vector of the tire is different from the heading of the tire. This can be caused by the steering angle δ and/or the yaw rate $\dot{\psi}$, e.g., during cornering. Longitudinal slip occurs when a braking or driving torque is applied to the wheel, e.g., during braking or acceleration.

There is a third slip quantity characterizing the whole vehicle. It's called the (vehicle) side slip β, which is defined as

$$\tan(\beta) = \frac{v_y}{v_x} \tag{3.3}$$

where v_x and v_y are the longitudinal and lateral velocities of the vehicle in a coordinate system attached to the vehicle.

A normal car has four wheels, which implies that there will be four tire slip angles, one for each wheel. To simplify the analysis, it is usually assumed that the front wheels have the same tire slip angle α_F, and that the rear wheels have the same angle α_R. The geometrical interpretation of α and β can be seen in Figure 3.1.

The longitudinal and lateral forces are in general dependent on four variables, $F_x = F_x(\alpha, \lambda, \gamma, F_z)$ and $F_y = F_y(\alpha, \lambda, \gamma, F_z)$, where α and λ are given in (3.1) respective (3.2), and F_z is the vertical normal force. The tire forces also depend on the camber angle γ, which is defined as the angle between the tilted wheel plane and the vertical plane. Therefore, the camber angle will depend on the roll angle φ of the vehicle and the steering angle δ. This dependence can be calculated according to (3.57).

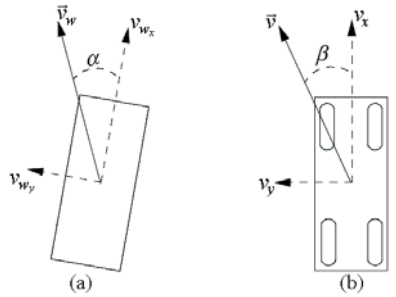

Figure 3.1: (a) shows the tire slip angle, the rectangle illustrates the tire. (b) shows the (vehicle) slip angle, the rectangle illustrates the vehicle.

3.1.1 Linear Force Model

The lateral force is the most important one during cornering. Figure 3.2 illustrates a typical relation between α and F_y with λ and F_z fixed. At small tire slip angles the relationship is approximately linear; the slope $C_{F\alpha}$ of the curve in this region is called the lateral slip stiffness or cornering stiffness. Therefore, the lateral force can be approximated by [11]

$$F_y = C_{F\alpha}\alpha \tag{3.4}$$

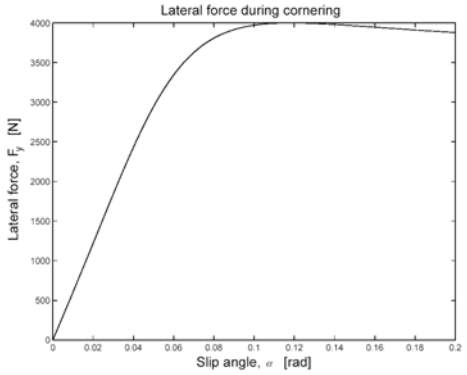

Figure 3.2: Lateral force versus slip angle during cornering, λ and F_z are fixed, [6].

3.1.2 Nonlinear Force Model

A general model that correctly describes the lateral and longitudinal forces under combined slip is complicated; therefore, a simplified model will be used. During pure lateral slip ($\lambda = 0$), the lateral force is at its maximum and the expression can be described by the Magic Formula, [11], which is shown in Figure 3.3. Note that it is the normalized force that is shown and the relationship between F_y and F_z is not linear. The saturation properties of the tire forces are also described in the formula. The parameters in the Magic Formula are described in Table 3.1; the actual parameters for a specific vehicle can be found through plotting the lateral force versus the slip angle and the normal force (as in Figure 3.3) from known data, and then analyzing this three-dimensional graph. The expression of the lateral force in the Magic Formula is [11]

$$F_y = F_y(\alpha, F_z) = D\sin(C\arctan(B\alpha - E(B\alpha - \arctan(B\alpha)))) \tag{3.5}$$

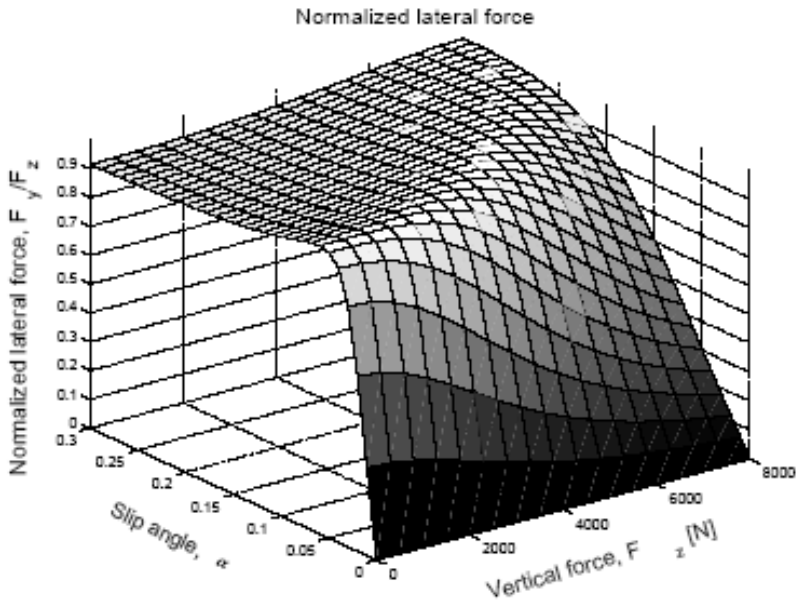

Figure 3.3: The Magic Formula: Normalized lateral force dependence on F_z and α, [6].

Parameter	Explanation
$B = \frac{C_{F\alpha}}{CD}$	Stiffness factor
C	Shape factor
$D = \mu F_z$	Peak factor
E	Curvature factor
$C_{F\alpha} = c_1 \sin(2 \arctan(\frac{F_z}{c_2}))$	Cornering stiffness
$c1$	Maximum cornering stiffness
$c2$	Load at maximum cornering stiffness

Table 3.1: Parameters in the Magic Formula.

When longitudinal slip is present the lateral force is described with $F_y = F_y(\alpha, \lambda, F_z)$, which can be expressed as $F_y = F_y(\alpha, F_x, F_z)$, since F_x depends on λ and F_x has a more direct physical meaning than λ.

The simplest model for combined slip, i.e., combined braking and cornering, is represented by the so-called friction ellipse. It is assumed that the forces F_x and F_y cannot exceed their maximum values, $F_{x_{max}}$ and $F_{y_{max}}$. The model is based on the resultant tire force is assumed to be on the edge of the friction ellipse during extreme maneuvers, e.g., cornering and braking. From the equation of an ellipse, $\left(\frac{F_y}{F_{y_{max}}(\alpha,F_z)}\right)^2 + \left(\frac{F_x}{F_{x_{max}}}\right)^2 = 1$, an expression for F_y can be derived. The maximum value $F_{y_{max}}(\alpha, F_z)$ is obtained when $\lambda = 0$, and could therefore be found by (3.5). [17] gives the maximum longitudinal force $F_{x_{max}} = \mu F_z$. The expression for the lateral force becomes

$$\begin{aligned} F_y &= \pm F_{y_{max}}(\alpha, F_z)\sqrt{1 - \left(\frac{F_x}{\mu F_z}\right)^2} \\ |F_x| &\leq \mu F_z \end{aligned} \tag{3.6}$$

The friction ellipse can be seen in Figure 3.4. Each wheel has its own friction ellipse, i.e, there exist four friction ellipses for a normal vehicle.

F_x is the only force the controller can influence directly, through braking. If the control law gives F_y, the corresponding longitudinal force F_x can be calculated using the friction ellipse (3.6) and the Magic Formula (3.5). The longitudinal slip λ that corresponds to a certain $F_x(\alpha, \lambda, F_z)$ can be calculated from using an approximated model of F_x, which is based on a fraction of two second order polynomials.

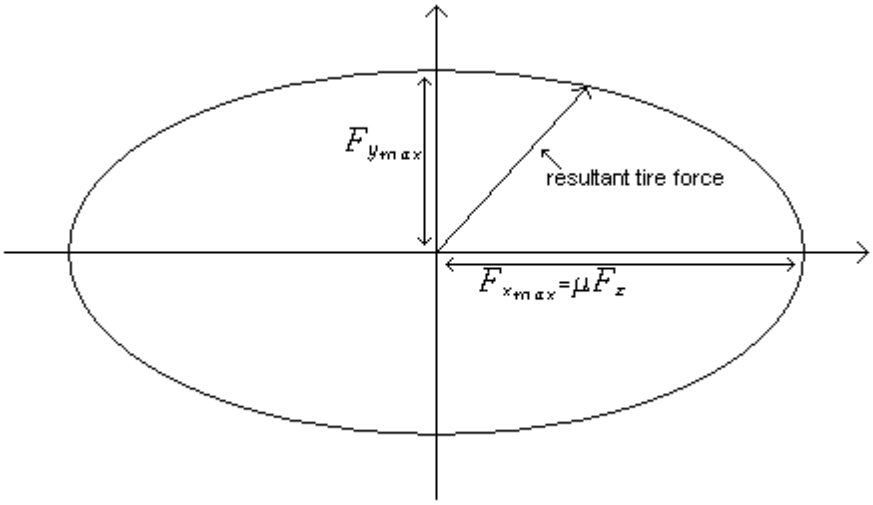

Figure 3.4: The friction ellipse for a tire. $F_{y_{max}}$ is given by (3.5).

3.1.3 Steerability

Three different cases describe the vehicle's steering behavior; understeering, neutral steering, and oversteering. According to the name, understeering indicates that the vehicle steers too less, which can result in that the vehicle drives off the road during cornering. If the vehicle stays on the road, understeering will stabilize the vehicle. On the other hand, oversteering indicates that the vehicle steers too much, which can make the vehicle unstable since the rollangle φ can increase rapidly.

According to [1], the steering behavior of the vehicle is defined by

$$\frac{d\delta}{da_y} > 0 \quad \Rightarrow \quad \text{understeering} \tag{3.7}$$

$$\frac{d\delta}{da_y} = 0 \quad \Rightarrow \quad \text{neutral steering} \tag{3.8}$$

$$\frac{d\delta}{da_y} < 0 \quad \Rightarrow \quad \text{oversteering} \tag{3.9}$$

where δ is the front wheel angle and a_y is the lateral acceleration of the vehicle. The steering behavior of the vehicle can be found by plotting the wheel angle δ as a function of the lateral acceleration a_y and examining the slope of the curve.

Under- or oversteering can be induced depending on which wheel the vehicle is braking during cornering. Figure 3.5 from [7] shows how the vehicle will steer during differential braking. When the yaw moment change is positive the vehicle will turn inward which induces oversteering. When it is negative the vehicle turns outward which induces understeering. As can be seen, braking on the inner wheels will always induce oversteering, which can make the vehicle unstable. Braking on the rear outer wheel results most of the time in understeering, but if the braking force becomes very large it can induce oversteering behavior. Braking on the front outer wheel will result in understeering of the vehicle, which will be stabilized.

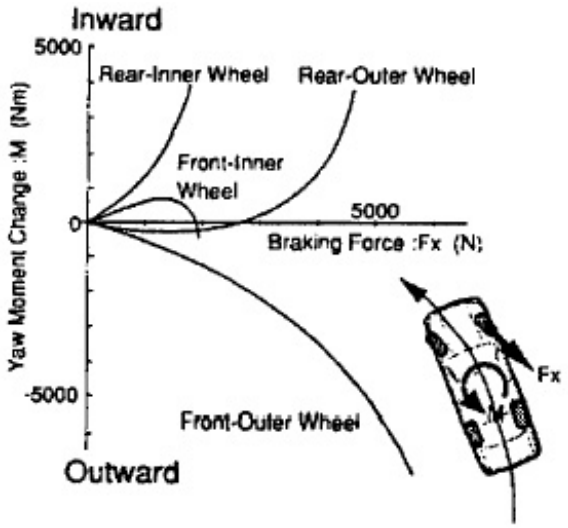

Figure 3.5: Yaw moment change as a function of braking force for each wheel.

3.2 Chassis Model

There are many different models used for characterizing the chassis of the vehicle. For example the Bicycle Model (the One-track Model), the Plane Model, the Two-track Model, and so on. They make different assumptions and simplifications, resulting in both linear and nonlinear equations of motion.

3.2.1 The Two-track Model

The brakes are the only control actuators. Braking on the outer track will stabilize the vehicle, therefore is it enough with a model assuming that the vehicle is on two wheels.

The nonlinear two-track model with roll dynamics gives a complete description of the rollover event for a vehicle. In this model the translational movement of the center of gravity in all directions, as well as the yaw and roll movement, are considered. The name *Two-track Model* should clarify that it is a result of the modeling of longitudinal, lateral, and yaw dynamics following the so-called simplified *One-track Model*, [12]. In difference from the one-track model, the single contact points of the tire forces and for this reason the track width are considered in the two-track model. This model assumes that the vehicle drives (during rolling) only on one track (two wheels); therefore there will only occur forces and momentum on the tires at this side.

The following simplifications are made

- no modeling of the spring and damper elements
- neglect the pitch dynamics
- approximately equal track widths $s = s_F = s_R$ (otherwise would the vehicle also pitch during rolling)
- the roll axis goes through the tire-contact center of the outside track.

Figure 3.6 shows the schematics of the modeled vehicle on two wheels. The vehicle has five degrees of freedom,

- the position of the center of gravity, $(x_{CoG}, y_{CoG}, z_{CoG})$
- the roll angle φ around the x-axis
- the yaw rate ψ around the z-axis.

One degree of freedom is lost due to the contact between the tires and the road surface, so the resulting four generalized coordinates are x_{CoG}, y_{CoG}, φ, and ψ. There are totally eight states,including the derivatives of the coordinates above. Five of these states are of interest here; namely the four velocities v_x, v_y, $\dot{\varphi}$, $\dot{\psi}$ as well as the roll angle φ.

The following derivation is mainly collected from [8].

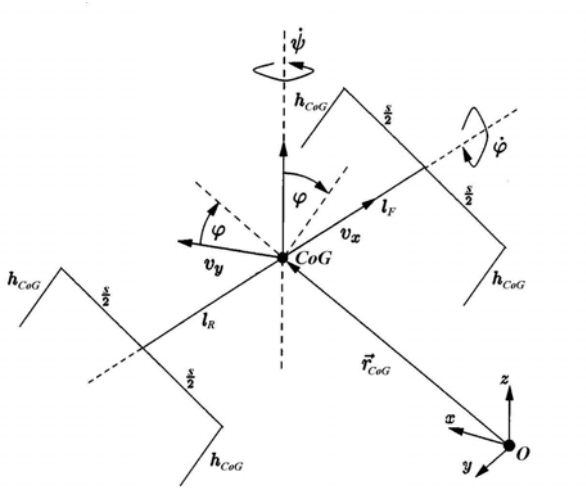

Figure 3.6: Representation of the two-track model with roll dynamics; the roll angle φ around the vehicle-attached x-axis.

Kinematics

Three coordinate systems are used to describe the vehicle motion. Besides the inertial system I and the vehicle-attached system K'', another moving, ψ rotated, horizontally coordinate system K' is defined. The vehicle's longitudinal velocity v_x, lateral velocity v_y, and yaw rate $\dot{\psi}$ are defined in the directions of this system, see Figure 3.7.

The rotation of the moving systems (K', K'') are defined through the following orthogonal transformation matrices

$$\boldsymbol{C}_{IK'} = \begin{pmatrix} \cos\psi & -\sin\psi & 0 \\ \sin\psi & \cos\psi & 0 \\ 0 & 0 & 1 \end{pmatrix} \tag{3.10}$$

$$\boldsymbol{C}_{K'K''} = \begin{pmatrix} 1 & 0 & 0 \\ 0 & \cos\varphi & -\sin\varphi \\ 0 & \sin\varphi & \cos\varphi \end{pmatrix} \tag{3.11}$$

K' is created through the rotation of I around the z-axis (yaw), K'' through another rotation around the x-axis (roll). The product of the matrices (3.10) and (3.11) gives the transformation from the inertial to the vehicle-attached

system

$$\boldsymbol{C}_{IK''} = \boldsymbol{C}_{IK'}\boldsymbol{C}_{K'K''} = \begin{pmatrix} \cos\psi & -\sin\psi\cos\varphi & \sin\psi\sin\varphi \\ \sin\psi & \cos\psi\cos\varphi & -\cos\psi\sin\varphi \\ 0 & \sin\varphi & \cos\varphi \end{pmatrix} \tag{3.12}$$

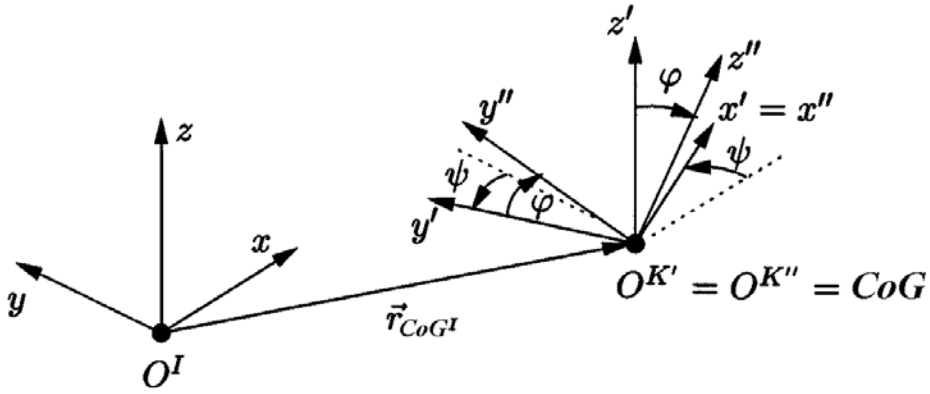

Figure 3.7: Three coordinate systems to describe the two-track model with roll dynamics: the inertial system I, the moving ψ-rotated horizontal system K', and the vehicle-attached (rolling) system K''.

According to [12] are the skew-symmetric tensors from I to K' respectively K'', represented in I, defined as

$$\tilde{\boldsymbol{\omega}}^I_{IK'} = \dot{\boldsymbol{C}}_{IK'}(\boldsymbol{C}_{IK'})^{\mathrm{T}} \tag{3.13}$$

$$\tilde{\boldsymbol{\omega}}^I_{IK''} = \dot{\boldsymbol{C}}_{IK''}(\boldsymbol{C}_{IK''})^{\mathrm{T}} \tag{3.14}$$

They contain the vectors of the rotational velocities; the vectors for the first rotation (yaw) are

$$\boldsymbol{\omega}^I_{IK'} = \boldsymbol{\omega}^{K'}_{IK'} = \begin{pmatrix} 0 \\ 0 \\ \dot{\psi} \end{pmatrix} \tag{3.15}$$

and the vectors for the rotation of the vehicle-attached system relative to the inertial one are

$$\boldsymbol{\omega}^I_{IK''} = \begin{pmatrix} \dot{\varphi}\cos\psi \\ \dot{\varphi}\sin\psi \\ \dot{\psi} \end{pmatrix} \text{ respectively } \boldsymbol{\omega}^{K''}_{IK''} = \begin{pmatrix} \dot{\varphi} \\ \dot{\psi}\sin\varphi \\ \dot{\psi}\cos\varphi \end{pmatrix} \tag{3.16}$$

The superscript indicates the coordinate system where the vector is represented.

The absolute velocity of the center of gravity CoG in the coordinate system K' is

$$\boldsymbol{v}_{CoG}^{K'} := \begin{pmatrix} v_x \\ v_y \\ v_z \end{pmatrix} \tag{3.17}$$

The acceleration of the center of gravity follows from the differentiation-rule of vectors in a moving coordinate system

$$\boldsymbol{a}_{CoG}^{K'} = \left(\frac{d^{K'}}{dt}\boldsymbol{v}_{CoG}\right)^{K'} + \boldsymbol{\omega}_{IK'}^{K'} \times \boldsymbol{v}_{CoG}^{K'} = \begin{pmatrix} \dot{v}_x - \dot{\psi}v_y \\ \dot{v}_y + \dot{\psi}v_x \\ \dot{v}_z \end{pmatrix} \tag{3.18}$$

$\dot{v}_x$, $\dot{v}_y$, and $\dot{v}_z$ denote the time-derivatives of the components of the velocity vector in the moving system K'.

Table 3.2 shows the indices for specific dimensions of the four contact points used in the following derivation. Since the contact points of the left track ($i = 1, 3$) does not carry any forces and momentum for positive roll angles $\varphi > 0$, it's enough to consider the contact points of the right track ($i = 2, 4$).

index	contact point
$i = 1$	front left
$i = 2$	front right
$i = 3$	rear left
$i = 4$	rear right

Table 3.2: Indices for the different contact points of the vehicle.

The position of the contact points in the vehicle-attached coordinate system K'' are described by

$$\boldsymbol{r}_2^{K''} = \begin{pmatrix} l_F \\ -\frac{s}{2} \\ -h_{CoG} \end{pmatrix} \text{ respectively } \boldsymbol{r}_4^{K''} = \begin{pmatrix} -l_R \\ -\frac{s}{2} \\ -h_{CoG} \end{pmatrix} \tag{3.19}$$

when the wheel caster and the steering offset are neglected. The assumption of an equal track width s in the front and rear is necessary since the

pitch motion is not modeled. The value of s is the mean values of the real widths s_F and s_R. By use of the abbreviations

$$h_0 = \sqrt{h_{CoG}^2 + \left(\frac{s}{2}\right)^2} \tag{3.20}$$

$$\varphi_0 = \arctan\left(\frac{2h_{CoG}}{s}\right) \tag{3.21}$$

the positions can be transformed into the horizontal coordinate system K'

$$\boldsymbol{r}_2^{K'} = \begin{pmatrix} l_F \\ -h_0\cos(\varphi+\varphi_0) \\ -h_0\sin(\varphi+\varphi_0) \end{pmatrix} \text{ respectively } \boldsymbol{r}_4^{K'} = \begin{pmatrix} -l_R \\ -h_0\cos(\varphi+\varphi_0) \\ -h_0\sin(\varphi+\varphi_0) \end{pmatrix} \tag{3.22}$$

The following differentiation rule are valid for the velocity of the contact points in K'

$$\boldsymbol{v}_i^{K'} = \boldsymbol{v}_{CoG}^{K'} + \boldsymbol{\omega}_{IK'}^{K'} \times \boldsymbol{r}_i^{K'} + \left(\frac{d^{K'}}{dt}\boldsymbol{r}_i\right)^{K'}, i = 2,4 \tag{3.23}$$

The velocities of the contact points can then be written as

$$\boldsymbol{v}_2^{K'} = \begin{pmatrix} v_x + h_0\dot{\psi}\cos(\varphi+\varphi_0) \\ v_y + l_F\dot{\psi} + h_0\dot{\varphi}\sin(\varphi+\varphi_0) \\ v_z - h_0\dot{\varphi}\cos(\varphi+\varphi_0) \end{pmatrix} \tag{3.24}$$

$$\boldsymbol{v}_4^{K'} = \begin{pmatrix} v_x + h_0\dot{\psi}\cos(\varphi+\varphi_0) \\ v_y - l_R\dot{\psi} + h_0\dot{\varphi}\sin(\varphi+\varphi_0) \\ v_z - h_0\dot{\varphi}\cos(\varphi+\varphi_0) \end{pmatrix} \tag{3.25}$$

If it is assumed that the contact points of the tires $i = 2$ and $i = 4$ always will have road contact then the z-components of $\boldsymbol{v}_2^{K'}$ and $\boldsymbol{v}_4^{K'}$ are equal to zero. This gives the z-component v_z of the velocity of the center of gravity

$$v_z = h_0\dot{\varphi}\cos(\varphi+\varphi_0) \tag{3.26}$$

with the time derivative

$$\dot{v}_z = h_0\ddot{\varphi}\cos(\varphi+\varphi_0) - h_0\dot{\varphi}^2\sin(\varphi+\varphi_0) \tag{3.27}$$

Derivation of the Model Equations

The equations of motion in the variables v_x, v_y, φ, and $\dot{\psi}$ for the two-track model with roll dynamics are derived in this section. The Newton/Euler laws are used.

Newton's second law in the horizontal moving coordinate system K' gives

$$m(\dot{v}_x - \dot{\psi} v_y) = F_{x,2} + F_{x,4} \tag{3.28}$$
$$m(\dot{v}_y + \dot{\psi} v_x) = F_{y,2} + F_{y,4} \tag{3.29}$$
$$m\dot{v}_z = F_{z,2} + F_{z,4} - mg \tag{3.30}$$

where $F_{x,i}$ respectively $F_{y,i}$ denote the sum of the tire forces (longitudinal and lateral forces) in the respective direction of the horizontal moving system K' at tire i. $F_{z,i}$ is the normal force at tire i.

The equation of angular momentum around the center of gravity in the vehicle attached system K'' is

$$\boldsymbol{J}_{CoG}^{K''} \dot{\boldsymbol{\omega}}_{IK''}^{K''} + \tilde{\boldsymbol{\omega}}_{IK''}^{K''} \boldsymbol{J}_{CoG}^{K''} \boldsymbol{\omega}_{IK''}^{K''} = \sum_i \boldsymbol{M}_{CoG,i}^{K''} \tag{3.31}$$

with $\boldsymbol{\omega}_{IK''}^{K''}$ from (3.16). A single differentiation gives

$$\dot{\boldsymbol{\omega}}_{IK''}^{K''} = \begin{pmatrix} \ddot{\varphi} \\ \ddot{\psi} \sin\varphi + \dot{\psi}\dot{\varphi}\cos\varphi \\ \ddot{\psi} \cos\varphi - \dot{\psi}\dot{\varphi}\sin\varphi \end{pmatrix} \tag{3.32}$$

$\tilde{\boldsymbol{\omega}}_{IK''}^{K''}$ is obtained through the following transformation of the tensor (3.14)

$$\tilde{\boldsymbol{\omega}}_{IK''}^{K''} = (\boldsymbol{C}_{IK''})^{\mathrm{T}} \tilde{\boldsymbol{\omega}}_{IK''}^{I} \boldsymbol{C}_{IK''} \tag{3.33}$$

The moment of inertia tensor in K'' is defined as

$$\boldsymbol{J}_{CoG}^{K''} = \begin{pmatrix} J_{xx} & 0 & 0 \\ 0 & J_{yy} & 0 \\ 0 & 0 & J_{zz} \end{pmatrix} \tag{3.34}$$

The angular momentum around the center of gravity comes from the tire forces in the two contact points and from the tire angular momenta in the z-direction of the inertial system

$$\sum_i \boldsymbol{M}_{CoG,i}^{K''} = \sum_{i=2,4} \left(\boldsymbol{r}_i^{K''} \times \boldsymbol{F}_i^{K''} + \boldsymbol{M}_i^{K''} \right) \tag{3.35}$$

where $\boldsymbol{r}_i^{K''}$ is the position of the contact point i in the system K'', see (3.19). The tire forces and angular momenta in K'' at the tires $i = 2, 4$ are

$$\boldsymbol{F}_i^{K''} = (\boldsymbol{C}_{K'K''})^{\mathrm{T}} \begin{pmatrix} F_{x,i} \\ F_{y,i} \\ F_{z,i} \end{pmatrix} \text{ respectively } \boldsymbol{M}_i^{K''} = (\boldsymbol{C}_{K'K''})^{\mathrm{T}} \begin{pmatrix} 0 \\ 0 \\ M_{z,i} \end{pmatrix} \tag{3.36}$$

Through combination of (3.31), (3.35), and (3.36) the angular momentum around the center of gravity in K'' yields

$$\begin{aligned} & J_{xx}\ddot{\varphi} + (J_{zz} - J_{yy})\dot{\psi}^2 \sin\varphi\cos\varphi \\ &= h_0 \sin(\varphi+\varphi_0)(F_{y,2}+F_{y,4}) - h_0\cos(\varphi+\varphi_0)(F_{z,2}+F_{z,4}) \end{aligned} \tag{3.37}$$

$$\begin{aligned} & J_{yy}(\ddot{\psi}\sin\varphi + \dot{\psi}\dot{\varphi}\cos\varphi) + (J_{xx} - J_{zz})\dot{\psi}\dot{\varphi}\cos\varphi \\ &= -h_{CoG}(F_{x,2}+F_{x,4}) + \sin\varphi(l_F F_{y,2} - l_R F_{y,4}) \\ &- \cos\varphi(l_F F_{z,2} - l_R F_{z,4}) + \sin\varphi(M_{z,2}+M_{z,4}) \end{aligned} \tag{3.38}$$

$$\begin{aligned} & J_{zz}(\ddot{\psi}\cos\varphi - \dot{\psi}\dot{\varphi}\sin\varphi) + (J_{yy} - J_{xx})\dot{\psi}\dot{\varphi}\sin\varphi \\ &= \tfrac{s}{2}(F_{x,2}+F_{x,4}) + \cos\varphi(l_F F_{y,2} - l_R F_{y,4}) \\ &+ \sin\varphi(l_F F_{z,2} - l_R F_{z,4}) + \cos\varphi(M_{z,2}+M_{z,4}) \end{aligned} \tag{3.39}$$

The normal forces $F_{z,2}$ and $F_{z,4}$ can be eliminated from the equations (3.28) to (3.30) and (3.37) to (3.39). Four differential equations for v_x, v_y, φ, and $\dot{\psi}$ are found by using the expression (3.27).

For the state vector

$$\boldsymbol{x} = \left(v_x \; v_y \; \varphi \; \dot{\varphi} \; \dot{\psi}\right)^{\mathrm{T}} \tag{3.40}$$

the following state space representation is obtained

$$\frac{dv_x}{dt} = \dot{\psi}v_y + \frac{1}{m}\left(F_{x,2}+F_{x,4}\right) \tag{3.41}$$

$$\frac{dv_y}{dt} = -\dot{\psi}v_x + \frac{1}{m}\left(F_{y,2}+F_{y,4}\right) \tag{3.42}$$

$$\frac{d\varphi}{dt} = \dot{\varphi} \tag{3.43}$$

$$\begin{aligned} \frac{d\dot{\varphi}}{dt} = & \frac{1}{J_{xx} + mh_0^2\cos^2(\varphi+\varphi_0)}\Big[\left(J_{yy}-J_{zz}\right)\dot{\psi}^2\sin\varphi\cos\varphi \\ & + mh_0^2\dot{\varphi}^2\sin(\varphi+\varphi_0)\cos(\varphi+\varphi_0) - mgh_0\cos(\varphi+\varphi_0) \\ & + h_0\sin(\varphi+\varphi_0)\left(F_{y,2}+F_{y,4}\right)\Big] \end{aligned} \tag{3.44}$$

$$\begin{aligned} \frac{d\dot{\psi}}{dt} = & \frac{1}{J_{yy}\sin^2\varphi + J_{zz}\cos^2\varphi}\Big[2\left(J_{zz}-J_{yy}\right)\dot{\psi}\dot{\varphi}\sin\varphi\cos\varphi \\ & + h_0\cos(\varphi+\varphi_0)\left(F_{x,2}+F_{x,4}\right) + l_F F_{y,2} - l_R F_{y,4} \\ & + M_{z,2} + M_{z,4}\Big] \end{aligned} \tag{3.45}$$

Assume the four dimensional input vector is

$$\boldsymbol{u} = \left(F_{x,2}\ F_{x,4}\ F_{y,2}\ F_{y,4}\right)^{\mathrm{T}} \tag{3.46}$$

and neglect the tire angular momenta $M_{z,2}$ and $M_{z,4}$. Then the state space model can be written in the input affine nonlinear form

$$\dot{\boldsymbol{x}} = \boldsymbol{f}(\boldsymbol{x}) + \sum_{i=1}^{4} \boldsymbol{g}_i(\boldsymbol{x}) u_i \tag{3.47}$$

The equations of motion for cornering to the right, i.e. with negative roll angle $\varphi < 0$, are obtained similarly to the above discussion (page 23 to 27). The following equations are obtained instead of (3.44) and (3.45)

$$\begin{aligned} \frac{d\dot{\varphi}}{dt} &= \frac{1}{J_{xx} + mh_0^2 \cos^2(\varphi - \varphi_0)} \Big[\left(J_{yy} - J_{zz}\right) \dot{\psi}^2 \sin\varphi \cos\varphi \\ &\quad + mh_0^2 \dot{\varphi}^2 \sin(\varphi - \varphi_0) \cos(\varphi - \varphi_0) + mgh_0 \cos(\varphi - \varphi_0) \\ &\quad - h_0 \sin(\varphi - \varphi_0) \left(F_{y,1} + F_{y,3}\right) \Big] \end{aligned} \tag{3.48}$$

$$\begin{aligned} \frac{d\dot{\psi}}{dt} &= \frac{1}{J_{yy} \sin^2\varphi + J_{zz} \cos^2\varphi} \Big[2 \left(J_{zz} - J_{yy}\right) \dot{\psi}\dot{\varphi} \sin\varphi \cos\varphi \\ &\quad - h_0 \cos(\varphi - \varphi_0) \left(F_{x,1} + F_{x,3}\right) + l_F F_{y,1} - l_R F_{y,3} \\ &\quad + M_{z,1} + M_{z,3} \Big] \end{aligned} \tag{3.49}$$

Extension of the Model Equations

The contact forces $F_{x,i}$ and $F_{y,i}$ are used in the derivation of the model equations. They are directed in the x- and y-direction of the vehicle, not the wheels. These forces can be related to the longitudinal $F_{x_w,i}$ and lateral $F_{y_w,i}$ forces at the wheels, i.e. in the wheels' coordinate systems, which are the actual forces that can be affected. Define the projection of the wheel angle δ_i in the horizontal plane as $\delta_{hor,i}$. Then

$$\delta_{hor,i} = \arctan(\cos\varphi \tan\delta_i) \tag{3.50}$$

for wheel number i. Then the following relationships can be derived.

$$F_{x,1} = F_{x_w,1} \cos\delta_{hor,1} + F_{y_w,1} \sin\delta_{hor,1} \tag{3.51}$$

$$F_{y,1} = -F_{x_w,1} \sin\delta_{hor,1} + F_{y_w,1} \cos\delta_{hor,1} \tag{3.52}$$

$$F_{x,2} = F_{x_w,2} \cos\delta_{hor,2} - F_{y_w,2} \sin\delta_{hor,2} \tag{3.53}$$

$$F_{y,2} = F_{x_w,2} \sin\delta_{hor,2} + F_{y_w,2} \cos\delta_{hor,2} \tag{3.54}$$

For the rear wheels the steering angles are zero and therefore $\delta_{hor,3,4} = 0$. This simplifies the relations to

$$F_{x,3} = F_{x_w,3} \ , \ F_{y,3} = F_{y_w,3} \tag{3.55}$$
$$F_{x,4} = F_{x_w,4} \ , \ F_{y,4} = F_{y_w,4} \tag{3.56}$$

The corresponding wheel forces $F_{x_w,i}$ and $F_{y_w,i}$ can be obtained through rearranging these equations. The longitudinal forces $F_{x_w,i}$ can be influenced directly if the internal dynamics are neglected. The lateral force $F_{y_w,i}$ depend on the tire slip angle α_i and therefore also on $\delta_{hor,i}$, on the camber angle γ_i, and on the slip λ_i at wheel i. From geometrically derivations it can be shown that the camber angle γ_i depends on the roll angle φ and the wheel angle δ_i as of

$$\gamma_i = \arcsin(\sin\varphi \cos\delta_i) \tag{3.57}$$

Since $\delta_3 = \delta_4 = 0$ the camber angle for the rear wheels can be simplified to $\gamma_3 = \gamma_4 = \varphi$. From the definition of the tire slip angle (3.1) and by consideration of the horizontal front wheel angle $\delta_{hor,i}$ the tire slip angles can be calculated through

$$\alpha_i = -\delta_{hor,i} + \arctan \frac{v_y + l_F\dot{\psi} + h_0\dot{\varphi}\sin(\varphi+\varphi_0)}{v_x + h_0\dot{\psi}\cos(\varphi+\varphi_0)} \ , \ i = 1,2 \tag{3.58}$$
$$\alpha_i = \arctan \frac{v_y - l_R\dot{\psi} + h_0\dot{\varphi}\sin(\varphi+\varphi_0)}{v_x + h_0\dot{\psi}\cos(\varphi+\varphi_0)} \ , \ i = 3,4 \tag{3.59}$$

Therefore the lateral forces have the following dependencies

$$F_{y_w,i} = F_{y_w,i}(\delta_i, \boldsymbol{x}) \ , \ i = 1,2 \tag{3.60}$$
$$F_{y_w,i} = F_{y_w,i}(\boldsymbol{x}) \ , \ i = 3,4 \tag{3.61}$$

which in general have nonlinear characteristics. Further, the adjustment of the wheel forces introduces delays. This so-called *breaking behavior* can be modeled with a PT_1-element, but that is not done in this thesis.

3.3 Vehicle Model

Combining the models (tires and chassis) discussed in this chapter will give a vehicle model that accurately enough describes its dynamics for rollover analysis.

The following relationships and properties can be obtained from the equations of motion (3.41) to (3.45), the section above (page 27-28), and from the friction ellipse seen in Figure 3.4.

- The lateral forces $F_{y,i}$ directly determine the lateral velocity v_y, the yaw rate $\dot{\psi}$, and the roll rate $\dot{\varphi}$.
- The longitudinal forces $F_{x,i}$ have direct influence on the longitudinal velocity v_x and the yaw rate $\dot{\psi}$.
- The longitudinal forces $F_{x,i}$ and the lateral forces $F_{y,i}$ on the same wheel are related according to the friction ellipse.
- Therefore, either lateral forces or longitudinal forces can be used to stabilize the roll dynamics.

The following chapters will examine the roll dynamics with respect to stability margins, detection, and prediction, as well as develop a control strategy to mitigate rollover.

Chapter 4

Rollover Detection

To be able to prevent rollover it is first necessary to predict and detect rollover. This chapter will outline two different ways to detect rollover before the vehicle actually flips.

4.1 Spring Deflections and Wheel Loads

When the vehicle is cornering it starts to tilt and load is transferred from the inner to the outer side of the curve. This means that the loads on the inner wheels are decreasing and the loads on the outer wheels are increasing. If the turn is sharp and the speed of the vehicle is high then the load transfer can become so large that one or both loads on the wheels on the inner side becomes zero, which implies that liftoff will occur and rollover is getting closer. Therefore, small wheel loads is an indication of possible rollover, which gives a way to detect it.

Static measurements are performed on a test vehicle; relating the spring deflections and the wheel loads on each wheel. Each side (left, right, front, rear) of the vehicle is gradually lifted, the spring deflections are noted, and the wheel loads are measured with scales under each tire. The tests show that there is a relationship between the spring deflections and the wheel loads. It is linear for "normal" loads (non-extreme maneuvers) and becomes nonlinear for extreme situations (the loads are close to zero or very large). This shows that, if the spring deflections can be measured, each wheel load can be calculated and rollover can be detected.

But, since today's commercial vans do not have spring deflection sensors, another strategy is needed to detect rollover.

4.2 Energy Description

By examining the roll energy of the vehicle, and compare it to a critical limit, rollover can be detected. [3] has been consulted in the derivation below.

Figure 4.1 shows an approximation of the vehicle as a rigid box connected to the ground via a rotational spring. In the example, mass is denoted m, J is the roll moment of inertia, c_φ is the roll stiffness, while s is the track width and h_{CoG} is the height of the center of gravity. Finally, φ denotes the roll angle. It is assumed that the rotational spring is at rest when $\varphi = 0$. The

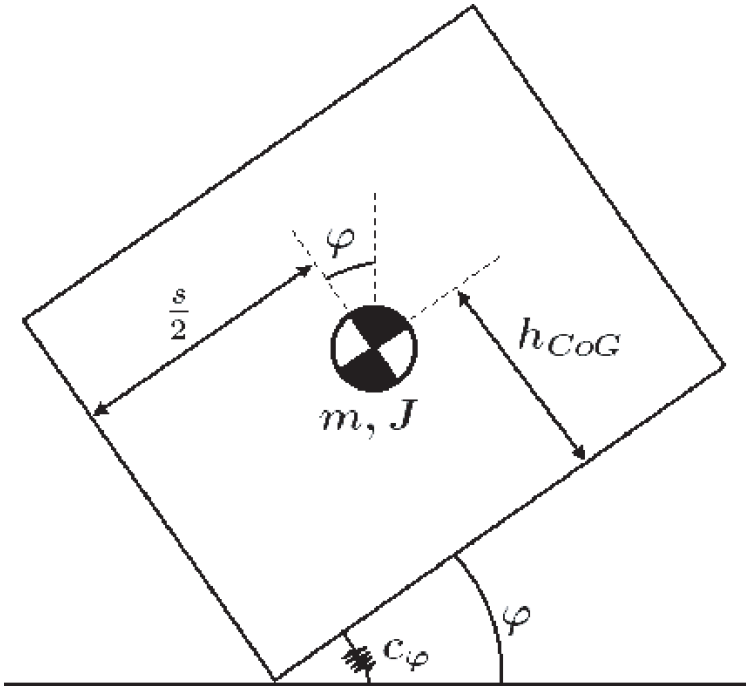

Figure 4.1: Rigid box example to illustrate the roll energy.

vehicle's roll energy consists of a potential and a kinetic part. The potential energy is

$$U = mg\left(\tfrac{s}{2}\sin\varphi + h_{CoG}(\cos\varphi - 1)\right) + \tfrac{1}{2}c_\varphi\varphi^2 \tag{4.1}$$

Hence, the potential energy is only depending on the roll angle φ and system-fixed parameters. Rollover is defined as occurring when the potential energy U reaches the critical potential energy U_{crit}. Since potential energy only depends on the roll angle φ, U_{crit} is found simply by deriving the angle φ_{crit} at which the derivative $dU/d\varphi = 0$.

The vehicle's kinetic roll energy is

$$T = \frac{1}{2} J_e \dot{\varphi}^2 = \frac{1}{2} \left(J + m \left((\frac{s}{2})^2 + h_{CoG}^2 \right) \right) \dot{\varphi}^2 \tag{4.2}$$

where $\dot{\varphi}$ is the roll rate. The kinetic energy depends only on the rate of change of the roll angle.

The energy margin E_Δ to rollover at any time is the difference between the critical potential energy (the energy needed to roll the vehicle) and the current sum of the potential and kinetic energy.

$$E_\Delta = U_{crit} - (U + T), \text{ where } U_{crit} = U(\varphi_{crit}) \tag{4.3}$$

If the energy margin is positive, the vehicle is stable and continues to oscillate around $\varphi = 0$, but if the margin is negative, rollover occurs unless stabilizing forces are applied. This gives a way to detect rollover if the roll angle φ and the roll rate $\dot{\varphi}$ are known.

Chapter 5

Rollover Mitigation

This chapter outlines a control system that mitigates rollover and skidding. It also shows tests and discusses the simulation results of the controller acting on the vehicle.

To have a big steering wheel angle is not dangerous itself, it is the kinetic and potential roll energy of the vehicle that is dangerous. Therefore, the main idea to prevent rollover is to lower the roll energy of the vehicle, which is done through allowing braking as the only actuation.

The vehicle is equipped with differential brakes, which allows the control system to brake on every wheel independently. Braking on the outer track during cornering will stabilize the vehicle.

5.1 Control Laws

The relationships for the used parameters h_0 (3.20) and φ_0 (3.21) in Chapter 3 can be rewritten as

$$\left.\begin{aligned} -h_0\cos(\varphi+\varphi_0) &= -\tfrac{s}{2}\cos\varphi + h_{CoG}\sin\varphi \\ h_0\sin(\varphi+\varphi_0) &= \tfrac{s}{2}\sin\varphi + h_{CoG}\cos\varphi \end{aligned}\right\} \quad \text{when} \quad \varphi > 0 \tag{5.1}$$

$$\left.\begin{aligned} h_0\cos(\varphi-\varphi_0) &= \tfrac{s}{2}\cos\varphi + h_{CoG}\sin\varphi \\ -h_0\sin(\varphi-\varphi_0) &= -\tfrac{s}{2}\sin\varphi + h_{CoG}\cos\varphi \end{aligned}\right\} \quad \text{when} \quad \varphi < 0 \tag{5.2}$$

These equations can easily be validated by a geometrical derivation. The following short-forms will be used during the derivation of the control

laws

$$\begin{aligned}\xi_\varphi(\dot\psi,\varphi,\dot\varphi) = \frac{1}{J_{xx}+m[\mp\frac{s}{2}\cos\varphi+h_{CoG}\sin\varphi]^2}\Big[&mg\big[\mp\frac{s}{2}\cos\varphi+h_{CoG}\sin\varphi\big]\\ &+\ \big(J_{yy}-J_{zz}\big)\dot\psi^2\sin\varphi\cos\varphi\\ &-\ m\dot\varphi^2\big[\mp\frac{s}{2}\cos\varphi+h_{CoG}\sin\varphi\big]\big[\pm\frac{s}{2}\sin\varphi+h_{CoG}\cos\varphi\big]\Big]\end{aligned} \tag{5.3}$$

$$\zeta_\varphi(\varphi) = \frac{\pm\frac{s}{2}\sin\varphi+h_{CoG}\cos\varphi}{J_{xx}+m[\mp\frac{s}{2}\cos\varphi+h_{CoG}\sin\varphi]^2} \tag{5.4}$$

$$\xi_\psi(\dot\psi,\varphi,\dot\varphi) = \frac{2(J_{zz}-J_{yy})\dot\psi\dot\varphi\sin\varphi\cos\varphi}{J_{yy}\sin^2\varphi+J_{zz}\cos^2\varphi} \tag{5.5}$$

$$\zeta_\psi(\varphi) = \frac{1}{J_{yy}\sin^2\varphi+J_{zz}\cos^2\varphi} \tag{5.6}$$

$$\zeta_x(\varphi) = \zeta_\psi\big[\pm h_{CoG}\cos(\varphi\pm\varphi_0)\big] = \zeta_\psi\Big[\pm\frac{s}{2}\cos\varphi-h_{CoG}\sin\varphi\Big] \tag{5.7}$$

The last equality is shown through using some simple algebra, and the relations (5.1) and (5.2). The ambiguous use of sign is because the upper sign is valid when the roll angle $\varphi > 0$, and the lower is valid when $\varphi < 0$. This makes the control laws valid at the same time for both positive and negative roll angles. An unambiguous representation is possible with the so-called signum-function, but this makes the overview of the terms less clear.

The following derivation is valid for both positive and negative roll angles φ and yaw rates $\dot\psi$, therefore a general designation for the forces on the outer wheels during cornering is needed since the two-track model is only assuming wheel contact on the outer side. Denote the longitudinal, lateral, and normal forces on the front outer wheel with $F_{x,F}$, $F_{y,F}$, and $F_{z,F}$. The forces on the rear wheel will be described by $F_{x,R}$, $F_{y,R}$, and $F_{z,R}$. Which side the forces correspond to is determined by the sign of the yaw rate $\dot\psi$ or the sign of the roll angle φ. So, if the yaw rate is positive $\dot\psi > 0$ the forces correspond to $F_{y,F} = F_{y,2}$, $F_{y,R} = F_{y,4}$ etc, and vice versa when the yaw rate is negative $\dot\psi < 0$; the wheel numbers are defined in Table 3.2.

The equations of motion (3.42) for v_y , (3.44) respectively (3.48) for $\dot\varphi$, and (3.45) respectively (3.49) for $\dot\psi$ are rewritten for both positive and negative roll angles $\varphi \in [-\frac{\pi}{2}, \frac{\pi}{2}]$ through use of the short-forms (5.3) to (5.7) and the

relationships (5.1) and (5.2), which yields

$$\dot{v}_y = -\dot{\psi}v_x + \frac{1}{m}\big[F_{y,F} + F_{y,R}\big] \tag{5.8}$$

$$\ddot{\varphi} = \xi_\varphi(\dot{\psi}, \varphi, \dot{\varphi}) + \zeta_\varphi(\varphi)\big[F_{y,F} + F_{y,R}\big] \tag{5.9}$$

$$\ddot{\psi} = \xi_\psi(\dot{\psi}, \varphi, \dot{\varphi}) + \zeta_\psi(\varphi)\big[l_F F_{y,F} - l_R F_{y,R}\big] + \zeta_x(\varphi)\big[F_{x,F} + F_{x,R}\big] \tag{5.10}$$

if the tire angular momenta $M_{z,F}$ and $M_{z,R}$ are neglected.
The time derivative of the lateral velocity $\dot{v}_y$ is related to the lateral acceleration a_y , the yaw rate $\dot{\psi}$, and the longitudinal velocity v_x through

$$\dot{v}_y = a_y - \dot{\psi}v_x \tag{5.11}$$

and it can be measured since a_y, $\dot{\psi}$, and v_x all are measurable. The lateral tire forces $F_{y,F}$ and $F_{y,R}$ in equation (5.9) and $F_{y,R}$, $F_{x,F}$, and $F_{x,R}$ in equation (5.10) are eliminated by insertion of (5.8), and by use of $ma_x = F_{x,F} + F_{x,R}$ and $ma_y = F_{y,F} + F_{y,R}$.

$$\ddot{\varphi} = \xi_\varphi(\dot{\psi}, \varphi, \dot{\varphi}) + \zeta_\varphi(\varphi)m\big[\dot{v}_y + \dot{\psi}v_x\big] \tag{5.12}$$

$$\ddot{\psi} = \xi_\psi(\dot{\psi}, \varphi, \dot{\varphi}) + \zeta_\psi(\varphi)\big[(l_F + l_R)F_{y,F} - l_R m a_y\big] + \zeta_x(\varphi)ma_x \tag{5.13}$$

To stabilize the roll, slip, and yaw dynamics the following Lyapunov function is proposed

$$V = \frac{1}{2}(\dot{\psi} - \dot{\psi}_{des})^2 + \frac{1}{2}c_1(\dot{\varphi} - \dot{\varphi}_{des})^2 + \frac{1}{2}c_2(\varphi - \varphi_{des})^2 + \frac{1}{2}c_3(v_y - v_{y_{des}})^2 \tag{5.14}$$

Assume that the constants $c_1, c_2, c_3 > 0$, then V is positive definite in the "error states" ($\boldsymbol{x} - \boldsymbol{x}_{des}$). The time derivative of the Lyapunov function $\dot{V}$ is

$$\begin{aligned}\dot{V} = {} & (\ddot{\psi} - \ddot{\psi}_{des})(\dot{\psi} - \dot{\psi}_{des}) + c_1(\ddot{\varphi} - \ddot{\varphi}_{des})(\dot{\varphi} - \dot{\varphi}_{des}) + c_2(\dot{\varphi} - \dot{\varphi}_{des})(\varphi - \varphi_{des}) \\ & + c_3(\dot{v}_y - \dot{v}_{y_{des}})(v_y - v_{y_{des}})\end{aligned} \tag{5.15}$$

Through rearrange of the $(\dot{\varphi} - \dot{\varphi}_{des})$-terms and by insertion of the equations (5.8), (5.12), and (5.13) the time derivative $\dot{V}$ becomes

$$\begin{aligned}\dot{V} = {} & \Big\{\xi_\psi(\dot{\psi}, \varphi, \dot{\varphi}) + \zeta_\psi(\varphi)\big[(l_F + l_R)F_{y,F} - l_R m a_y\big] + \zeta_x(\varphi)ma_x - \ddot{\psi}_{des}\Big\} \\ & (\dot{\psi} - \dot{\psi}_{des}) + \Big\{c_1\Big[\xi_\varphi(\dot{\psi}, \varphi, \dot{\varphi}) + \zeta_\varphi(\varphi)m\big[\dot{v}_y + \dot{\psi}v_x\big] - \ddot{\varphi}_{des}\Big] + c_2(\varphi - \varphi_{des})\Big\} \\ & (\dot{\varphi} - \dot{\varphi}_{des}) + \Big\{c_3\Big[-\dot{\psi}v_x + \frac{1}{m}\big[F_{y,F} + F_{y,R}\big] - \dot{v}_{y_{des}}\Big]\Big\}(v_y - v_{y_{des}})\end{aligned} \tag{5.16}$$

and at last

$$\begin{aligned}\dot{V} = &\Big\{\underbrace{\xi_\psi(\dot{\psi},\varphi,\dot{\varphi}) + \zeta_\psi(\varphi)\big[(l_F+l_R)F_{y,F} - l_R m a_y\big] + \zeta_x(\varphi) m a_x - \ddot{\psi}_{des}}_{term_1}\Big\}\\ &(\dot{\psi}-\dot{\psi}_{des}) + \Big\{\underbrace{c_1\Big[\xi_\varphi(\dot{\psi},\varphi,\dot{\varphi}) + \zeta_\varphi(\varphi) m\big[\dot{v}_y + \dot{\psi}_{des} v_x\big] - \ddot{\varphi}_{des}\Big] + c_2(\varphi-\varphi_{des})}_{term_2}\Big\}\\ &(\dot{\varphi}-\dot{\varphi}_{des}) + c_1 m v_x \zeta_\varphi(\varphi)(\dot{\psi}-\dot{\psi}_{des})(\dot{\varphi}-\dot{\varphi}_{des})\\ &+ \Big\{\underbrace{c_3\Big[-\dot{\psi}v_x + \frac{1}{m}\big[F_{y,F}+F_{y,R}\big] - \dot{v}_{y_{des}}\Big]}_{term_3}\Big\}(v_y - v_{y_{des}})\end{aligned} \tag{5.17}$$

Define the following equalities

$$term_1 = -\lambda_1(\dot{\psi}-\dot{\psi}_{des}) \tag{5.18}$$
$$term_2 = -\lambda_2(\dot{\varphi}-\dot{\varphi}_{des}) \tag{5.19}$$
$$term_3 = -\lambda_3(v_y - v_{y_{des}}) \tag{5.20}$$

Then $\dot{V}$ can be simplified to

$$\begin{aligned}\dot{V} = &-\lambda_1(\dot{\psi}-\dot{\psi}_{des})^2 - \lambda_2(\dot{\varphi}-\dot{\varphi}_{des})^2 + c_1 m v_x \zeta_\varphi(\varphi)(\dot{\psi}-\dot{\psi}_{des})(\dot{\varphi}-\dot{\varphi}_{des})\\ &-\lambda_3(v_y - v_{y_{des}})^2\end{aligned} \tag{5.21}$$

which can be rearranged to

$$\begin{aligned}\dot{V} = &-\big[\lambda_1 - \frac{1}{2}c_1 m v_x \zeta_\varphi(\varphi)\big](\dot{\psi}-\dot{\psi}_{des})^2 - \big[\lambda_2 - \frac{1}{2}c_1 m v_x \zeta_\varphi(\varphi)\big](\dot{\varphi}-\dot{\varphi}_{des})^2\\ &-\frac{1}{2}c_1 m v_x \zeta_\varphi(\varphi)\big[(\dot{\psi}-\dot{\psi}_{des}) - (\dot{\varphi}-\dot{\varphi}_{des})\big]^2 - \lambda_3(v_y - v_{y_{des}})^2\end{aligned} \tag{5.22}$$

If the following relationships are satisfied

$$\lambda_i > \frac{1}{2}c_1 m v_x \zeta_\varphi(\varphi),\ i=1,2 \tag{5.23}$$
$$\frac{1}{2}c_1 m v_x \zeta_\varphi(\varphi) > 0,\ \text{true since } c_1, m, v_x, \zeta_\varphi(\varphi) > 0 \text{ if } \varphi \in [-\tfrac{\pi}{2}, \tfrac{\pi}{2}] \tag{5.24}$$
$$\lambda_3 > 0 \tag{5.25}$$

$\dot{V}$ will become negative semi-definite in the error states $z_1 = (\dot{\psi}-\dot{\psi}_{des})$, $z_2 = (\dot{\varphi}-\dot{\varphi}_{des})$, $z_3 = (\varphi-\varphi_{des})$, and $z_4 = (v_y - v_{y_{des}})$. It will only become semi-definite since the state z_3 is not present in (5.22).

Since V (5.14) is also a scalar, radially unbounded, and continuously differentiable function of the states it fulfills the assumptions of Theorem 2.2 and therefore are the error states z_1, z_2, and z_4 stable around the origin. Since z_3 is not present in (5.22) it has to be shown that also z_3 is stable around the origin when the other error states are stable. That will be done further on.

Equations (5.18) to (5.20) are used to find the control signals that stabilizes the error states. To control the yaw rate $\dot{\psi}$ equation (5.18) is used

$$\xi_\psi(\dot{\psi},\varphi,\dot{\varphi})+\zeta_\psi(\varphi)\big[(l_F+l_R)F_{y,F}-l_R m a_y\big]+\zeta_x(\varphi)ma_x-\ddot{\psi}_{des}=-\lambda_1(\dot{\psi}-\dot{\psi}_{des}) \tag{5.26}$$

Solving for $F_{y,F}$ results in the following control law for $\dot{\psi}$

$$\begin{aligned}F_{y,F}=\frac{1}{\zeta_\psi(\varphi)(l_F+l_R)}\Big[&-\xi_\psi(\dot{\psi},\varphi,\dot{\varphi})+\zeta_\psi(\varphi)l_R m a_y-\zeta_x(\varphi)ma_x+\ddot{\psi}_{des}\\&-\lambda_1(\dot{\psi}-\dot{\psi}_{des})\Big]\end{aligned} \tag{5.27}$$

Equation (5.19) is used to control the roll angle φ and the roll rate $\dot{\varphi}$.

$$c_1\Big[\xi_\varphi(\dot{\psi},\varphi,\dot{\varphi})+\zeta_\varphi(\varphi)m\big[\dot{v}_y+\dot{\psi}_{des}v_x\big]-\ddot{\varphi}_{des}\Big]+c_2(\varphi-\varphi_{des})=-\lambda_2(\dot{\varphi}-\dot{\varphi}_{des}) \tag{5.28}$$

Rearranging and using (5.11) gives

$$c_1\zeta_\varphi(\varphi)mv_x\left[\frac{a_y}{v_x}-\dot{\psi}+\dot{\psi}_{des}\right]=-c_1\xi_\varphi(\dot{\psi},\varphi,\dot{\varphi})+c_1\ddot{\varphi}_{des}-c_2(\varphi-\varphi_{des})-\lambda_2(\dot{\varphi}-\dot{\varphi}_{des}) \tag{5.29}$$

Finally, solving for $\dot{\psi}_{des}$ gives the control law that governs the roll dynamics corresponding to φ and $\dot{\varphi}$

$$\begin{aligned}\dot{\psi}_{des}=\dot{\psi}+\frac{1}{c_1\zeta_\varphi(\varphi)mv_x}\Big[&-c_1\big[\xi_\varphi(\dot{\psi},\varphi,\dot{\varphi})+\zeta_\varphi(\varphi)ma_y-\ddot{\varphi}_{des}\big]-c_2(\varphi-\varphi_{des})\\&-\lambda_2(\dot{\varphi}-\dot{\varphi}_{des})\Big]\end{aligned} \tag{5.30}$$

The stability of the error state $z_3=(\varphi-\varphi_{des})$ can now easily be shown. As proved above, assume that the other error states are stable around the origin, i.e. $z_1=z_2=z_4=0$. By identifying $\ddot{\varphi}$ in (5.30) using (5.12) and (5.11) two error states are left. Letting the desired value of the roll acceleration $\ddot{\varphi}_{des}$ be equal to the actual acceleration $\ddot{\varphi}$ it shows that $z_3=(\varphi-\varphi_{des})=0$, i.e. the error state of the roll angle is also stable around the origin.

The last control law, which controls the lateral velocity v_y and therefore the side slip β, is obtained through use of equation (5.20)

$$c_3\left[-\dot{\psi}v_x + \frac{1}{m}\left[F_{y,F} + F_{y,R}\right] - \dot{v}_{y_{des}}\right] = -\lambda_3(v_y - v_{y_{des}}) \tag{5.31}$$

Solving for $F_{y,R}$ results in a control law that controls v_y

$$F_{y,R} = -F_{y,F} + m\left[\dot{\psi}v_x + \dot{v}_{y_{des}} - \frac{\lambda_3}{c_3}(v_y - v_{y_{des}})\right] \tag{5.32}$$

where $F_{y,F}$ is already known from the control law (5.27).

5.2 Controller Design

The controller is implemented in Matlab as an S-function, which is used in a Simulink model to simulate the vehicle. Figure 5.1 shows the main view of the model with all the different parts using a sample time of 1 ms.

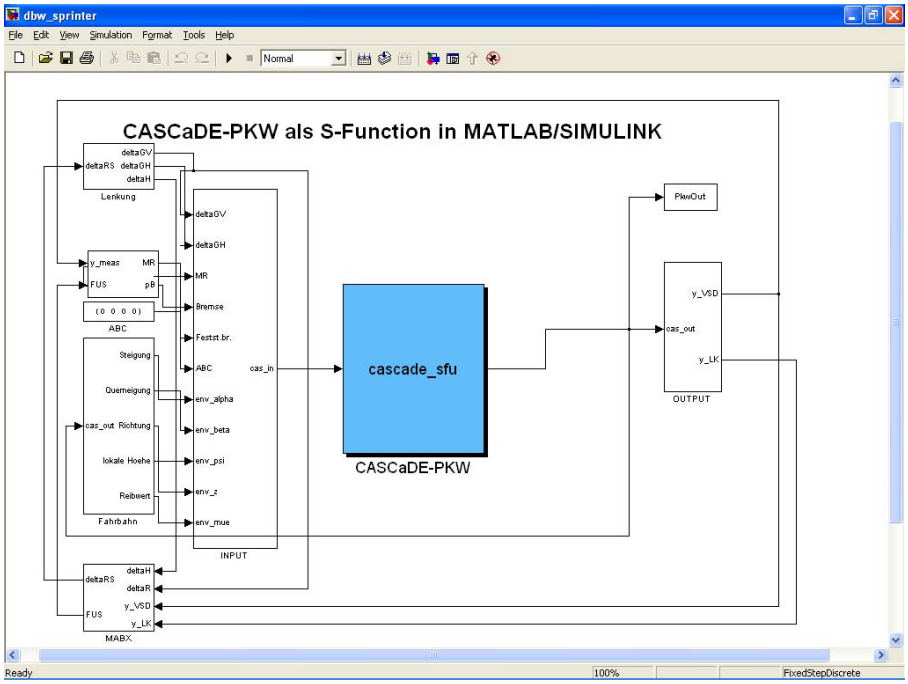

Figure 5.1: Simulink model for simulation of the vehicle.

The main part is the modeling of the vehicle in CASCaDE, where lookup-tables are used to get the output signals through using the input values. The boxes to the left in Figure 5.1 are used to calculate the input signals (steering angle, brake torques, road parameters etc.) to the CASCaDE vehicle model. The upper most box governs the steering wheel input, which defines the actual maneuver. It gives the steering wheel angle as a function of time, i.e. there is no defined road since the velocities can be different for different vehicles or maneuvers.

The box at the bottom to the left in Figure 5.1 contains the Lyapunov controller (see Figure 5.2), which controls the roll motion and the side slip. The controller calculates the longitudinal braking forces on each wheel needed to stabilize the vehicle. They are then given as outputs from the S-function (*sfdlyap.m*). The braking forces are sent to the second most upper box in

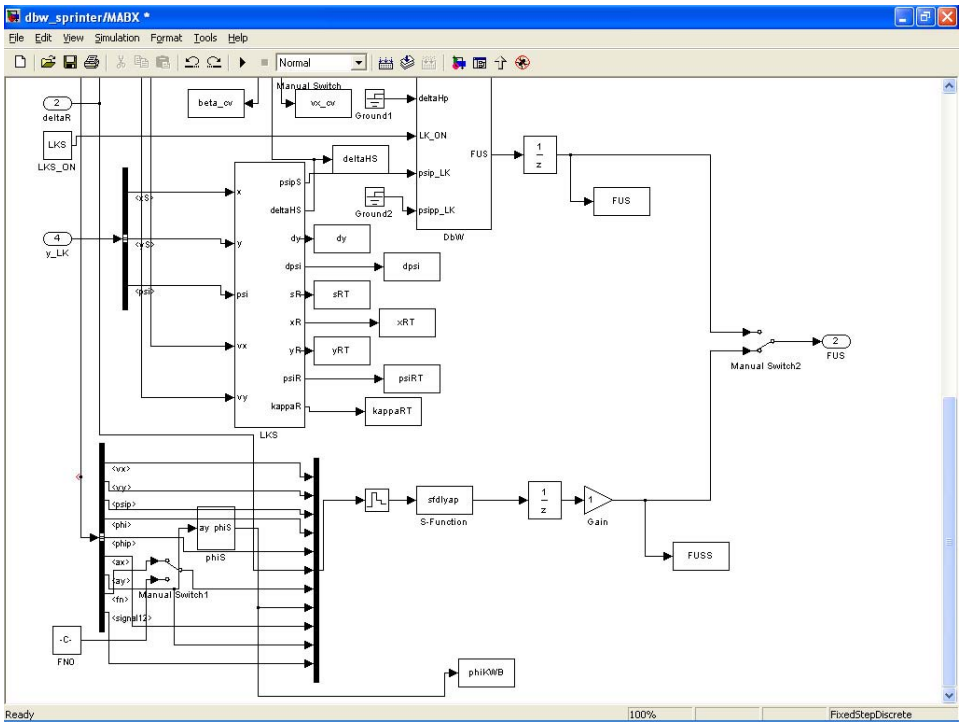

Figure 5.2: The part of the Simulink model which contains the Lyapunov controller, called *sfdlyap*.

Figure 5.1. There are they converted to braking torques through using the ABS[1]. The torques are then sent to the CASCaDE vehicle model as inputs.

[1] Anti-lock Brake System

The inputs to the Lyapunov controller can be seen in Figure 5.2. It needs the longitudinal velocity v_x and acceleration a_x, the lateral velocity v_y and acceleration a_y, the yaw rate $\dot{\psi}$, the roll angle φ and the roll rate $\dot{\varphi}$, the normal forces $F_{z,i}$ on each wheel, and the steering angle δ. All these states are assumed to be known from the CASCaDE vehicle model. Since it is only allowed to brake when mitigating rollover and skidding, the controller simply gives the braking force on each wheel as outputs.

The structure of the S-function that acts as a Lyapunov controller is as follows (it will be discussed intensively below);

- set some physical constants, margins, and vehicle load parameters
- load the inputs (see the discussion above and Figure 5.2)
- check how the vehicle is cornering (to the left or to the right) and compute needed vehicle characteristics, i.e. slip quantities, camber angles etc.
- set the desired values, i.e. $\beta_{des}, \dot{\beta}_{des}, \varphi_{des}, \dot{\varphi}_{des}, \ddot{\varphi}_{des}, \ddot{\psi}_{des}$
- do rollover and skidding detection
- control the vehicle if needed; set up some short forms and controller constants, calculate the control laws (i.e. the desired yaw rate $\dot{\psi}_{des}$ and the lateral forces $F_{y,F}, F_{y,R}$)
- use an advanced Magic Formula (C-function) to get the maximum tire forces and then convert the lateral forces to longitudinal braking forces through use of the friction ellipse
- set the longitudinal forces on each wheel as outputs from the S-function, if there is no detection of rollover or skidding the outputs are set to zero.

The margins (for rollover and side slip detection) are minimized to show the limits of the controller. Of course, in a future controller, these margins will be tuned for best performance of the vehicle. The load parameters in the controller specifies the mass and moments of inertia of the vehicle and the position of the center of gravity. Since these parameters are unknown and cannot be measured in today's vehicles they have to be estimated. As shown below in section 5.4.2 the controller can assume that the vehicle is fully loaded even though it might not be. So the load parameters in the

controller are always set to those for the fully loaded vehicle; they can be seen in Appendix A.

How the vehicle is cornering (to the left or to the right) and rolling is simply determined from the sign of the yaw rate, see page 13. The vehicle characteristics are computed as described in (3.3), (3.50), (3.57), (3.58), and (3.59).

The desired values for the side slip β_{des} and $\dot{\beta}_{des}$ are set as in the source code for the ESP system. Basically, a β_{max} depending on the velocity v_x is calculated and compared to the actual side slip β. The desired value is obtained through setting $\beta_{des} = \min(\max(-\beta_{max}, \beta), \beta_{max})$. So the desired value is something in between the limit values $\pm\beta_{max}$, or equal to one of the limits depending on the magnitude of the actual side slip β. As stated before, a minimized safety margin is used when applying these limits. Skidding is detected if the magnitude of the side slip is outside this region. β_{max} is in between 3° and 10° depending on the velocity (e.g. 90 km/h gives a maximum side slip of $\beta_{max} = 7.3^\circ$). The derivative of the side slip $\dot{\beta}_{des}$ is computed in two different ways depending on if the actual side slip β is outside the region $\pm\beta_{max}$ or not. $\ddot{\psi}_{des}$ is simply set to zero since the yaw rate only contains first order dynamics.

The same approach as for β_{des} is used when setting the desired roll angle φ_{des}. φ_{des} is equal to the actual roll angle φ as long as it is inside a region limited by the critical roll angle φ_{crit}, defined on page 33. The desired roll angle φ_{des} is equal to $\pm\varphi_{crit}$ (approximately $\pm 6^\circ$) when the actual angle is outside this region. A minimized safety margin is also used when setting the limits of this region. The settings of $\dot{\varphi}_{des}$ and $\ddot{\varphi}_{des}$ depend on if rollover is detected or not. Three different criterions are used to detect rollover. The actual roll angle φ is compared to the critical roll angle φ_{crit}. Since the roll angle only governs the potential energy, another criterion is needed to cover the kinetic part. The roll rate $\dot{\varphi}$ is therefore compared to a preset maximum value. Finally, to cover the intermediate cases the total roll energy is compared to the critical potential energy, see (4.1), (4.2), and (4.3). Different safety margins are used to predict and detect rollover on time. If rollover is detected $\dot{\varphi}_{des}$ is set so it directs φ and $\dot{\varphi}$ back into the safe region, where no rollover can take place. $\ddot{\varphi}_{des}$ is then defined as the difference between the desired roll rate $\dot{\varphi}_{des}$ and the actual roll rate $\dot{\varphi}$, which is a measurement of the roll acceleration. If rollover is not detected nothing needs to be done, so simply setting $\dot{\varphi}_{des} = \dot{\varphi}$ and $\ddot{\varphi}_{des} = 0$ is enough.

The shorts forms (5.3) to (5.7) are used when the control laws are calcu-

lated. The controller constants are chosen, see section 5.4.1 below, so the constraints on the constants are satisfied, i.e. (5.23), (5.25), and $c_1, c_2, c_3 > 0$. The yaw rate $\dot{\psi}_{des}$, which controls the roll motion, is calculated using (5.30). This yaw rate is then used when the lateral force on the front outer wheel $F_{y,F}$ is determined through using (5.27). To control the side slip the lateral force on the rear outer wheel $F_{y,R}$ is calculated according to (5.32).

A complex Magic Formula (see page 16) is used to get the maximum tire forces for a specific μ, $F_{z,i}$, λ_i, α_i, and γ_i. This formula is a C-function taken from the ESP source code with the variables above as inputs. Then the lateral forces are converted to longitudinal braking forces through using the so-called friction ellipse (see page 17). The front longitudinal force is converted from the vehicle coordinate system to the tire coordinate system using (3.51) to (3.54).

Finally, the calculated longitudinal braking forces on the outer track during cornering are set as outputs from the S-function. If no rollover and no skidding are detected the outputs are just set to zero, because the vehicle is not in a critical position so there is no need for braking.

5.3 Simulation Tests

The Simulink model of the controller and the vehicle is tested for different maneuvers, initial velocities, and load conditions. The maneuver is defined by the steering wheel angle as a function of time; i.e. there is no defined road. The vehicle is simulated for velocities up to 140 km/h and two load cases are tested; empty vehicle and fully loaded vehicle, see Appendix A.

Five different maneuvers are examined; ramp (linearly increasing steering angle), chirp (sinusoidal with linearly increasing frequency), sinusoidal (constant frequency), step, and fishhook. The fishhook is a step to the left and then a longer step to the right followed by constant angle for a while and finally a ramp back to the initial steering angle. Every maneuver is simulated for 10 s.

Time-plots are constructed for the most important vehicle parameters, e.g. wheel angle δ, yaw rate $\dot{\psi}$, roll angle φ, roll rate $\dot{\varphi}$, slip angle β, lateral acceleration a_y, longitudinal velocity v_x, and tire forces $F_{x,i}$, $F_{y,i}$, $F_{z,i}$. The wheel angle δ versus the lateral acceleration a_y are also plotted for stationary motion.

The Lyapunov controller is compared to an already existing LQ-controller and a vehicle without any roll or skid control at all. Comparisons are done through examining the plots and through use of video animations of the test-runs.

5.4 Simulation Results and Discussions

This section shows and discusses the results from the simulations. First the controller is tuned and then the robustness is discussed. The performance of the Lyapunov controller is examined using plots and animations. Finally, the controller is compared to an already existing LQ-controller.

5.4.1 Tuning

Before the controller can be tested and used intensively it needs to be tuned. Controller constants, safety margins etc. are tuned to make the controller perform better. The parameters are tuned so the controller works well for all the different maneuvers (see section 5.3), different velocities, and load conditions.

Tests show that the best set of controller constants are

$$c_1 = 0.5,\ c_2 = 40,\ c_3 = 1,\ \lambda_{1,2} = 0.6c_1 m v_x \zeta_\varphi(\varphi),\ \lambda_3 = 2 \tag{5.33}$$

These constants satisfies the constraints on them, i.e. (5.23), (5.25), and $c_1, c_2, c_3 > 0$.

The safety margins for the setting of the desired states are minimized to show the limits of the controller.

5.4.2 Controller Robustness against Uncertain Load Conditions

The position of the center of gravity and the vehicle's mass are coupled. When the mass increases the position moves most of the time backwards and up. The only exception is when the vehicle is loaded with for example a flat block of lead on the floor, but this will just stabilize the vehicle.

The controller cannot know the actual load case ($m, h_{CoG}, l_F, l_R, J_{xx}, J_{yy}, J_{zz}$) in the vehicle. Either must these parameters be estimated with an adaptive part, which estimates one or a few of them and then calculates the rest from the coupling, or if the controller is robust it can assume that the load case is the same all the time even though it might not be.

Simulations show that when the controller assumes that the vehicle is fully loaded it works better than if it assumes that the vehicle is loaded with a mean between full and empty. There is no significant difference between the performance of the controller assuming full load compared to the controller that knows the exact load condition. This shows that the controller is robust against uncertainties in the load conditions. Therefore, no adaptive part, which would have slowed down the controller, is needed. From now on will the controller always assume that the vehicle is fully loaded (see Appendix A for load parameters), even though it might not be. Simulations of this controller show that the magnitude of the yaw rate and the lateral acceleration is allowed to be bigger for lighter vehicles; showing that the controller works properly.

5.4.3 General Evaluation of the Lyapunov Controller

Maneu.	Load	Steering wheel angle or rate, freq.	max $v_{x,0}$ [km/h]
ramp	empty	$45°$/s up to $180°$/s	140 and more
ramp	full	$45°$/s up to $180°$/s	140 and more
chirp	empty	$135°, 0.1 \rightleftharpoons 2, 0.4 \rightleftharpoons 0.8, 0.01 \rightarrow 1$ Hz	140 and more
chirp	full	$135°, 0.1 \rightleftharpoons 2, 0.4 \rightleftharpoons 0.8, 0.01 \rightarrow 1$ Hz	nice up to 120
sinus	empty	$135°, 0.5, 0.01, 0.1, 0.4, 0.6, 0.7$ Hz	140 and more
sinus	full	$135°, 0.5, 0.01, 0.1, 0.4, 0.6, 0.7$ Hz	nice up to 120
step	empty	$200°$ and $400°$	140 and more
step	full	$200°$ and $400°$	140 and more
fishhook	empty	standard, maximum at $162.5°$	ok up to 130
fishhook	full	standard, maximum at $162.5°$	nice up to 120

Table 5.1: The controller works well for these maneuvers, load conditions, and maximum initial velocities.

The vehicle governed by the Lyapunov controller is tested for the maneuvers, maximum velocities, and load conditions shown in Table 5.1. The steering wheel angles, rates, and frequencies given in the table are tested

up to the maximum velocities given in the rightmost column. The vehicle is avoiding rollover and skidding (stays inside the limit values $\pm\beta_{max}$ and $\pm\varphi_{crit}$) at least up to these values. The table shows that the Lyapunov controller works good for extreme maneuvers and high speeds. The controller is also tested for normal driving maneuvers showing that it will not affect them by applying braking forces unless rollover or skidding is close.

Numerous plots and animations of the maneuvers show the behavior of the vehicle. Both the full and empty vehicle have a roll eigenfrequency that is approximately 0.5 Hz, which is validated by simulating a vehicle without a controller using a sinusoidal steering input.

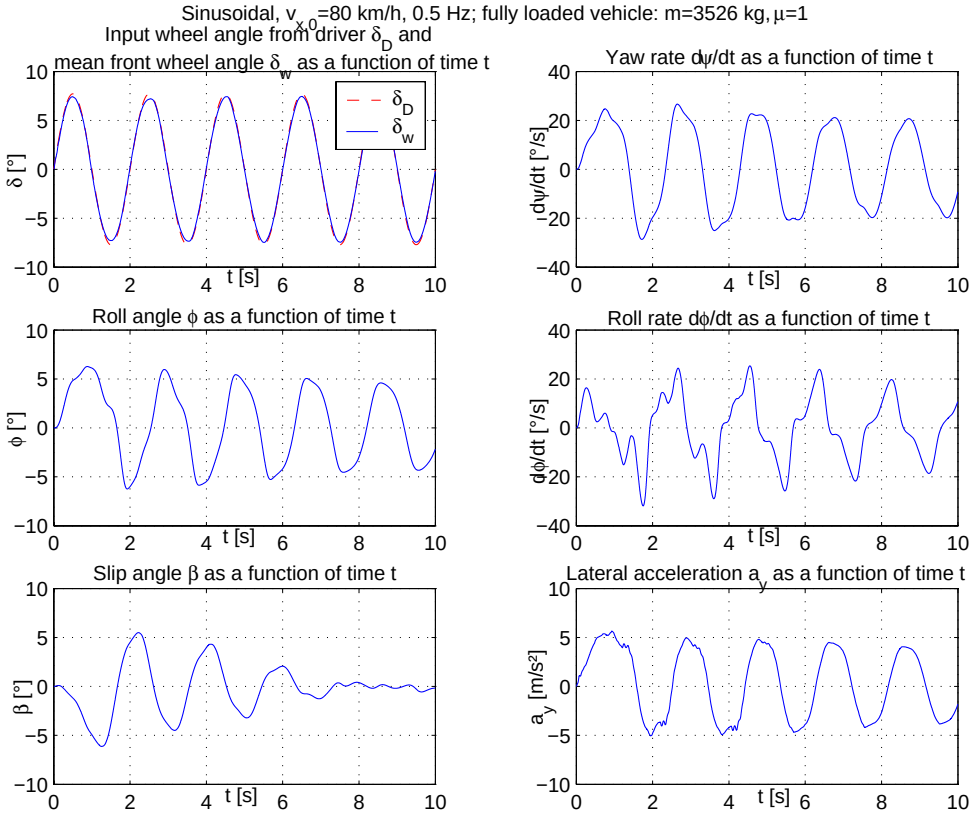

Figure 5.3: Plots from simulation with a sinusoidal steering input (135° and 0.5 Hz) for a fully loaded vehicle in 80 km/h using the Lyapunov controller that assumes full load.

Figure 5.3 illustrates the simulation of a 0.5 Hz sinusoidal input signal to show if the controller stabilizes the vehicle around the eigenfrequency.

The amplitude on the steering wheel is $135°$, which gives a front wheel angle of approximately $7.7°$ since the ratio between the steering wheel and the wheels are 17.5 for the commercial van; this extreme maneuver can be seen in the left uppermost plot. The right uppermost plot of the yaw rate $\dot{\psi}$ shows that the vehicle follows the desired input path well. The roll angle φ and the side slip β stay most of the time inside their limit values, and they decrease by time. The roll rate $\dot{\varphi}$ is pretty large since it is a sinusoidal signal, but the control on it is enough to stabilize the vehicle. The lateral acceleration reaches a little above 5 m/s^2 for the fully loaded vehicle. Also the animation of the vehicle shows how it is well controlled and no rolling or skidding is present.

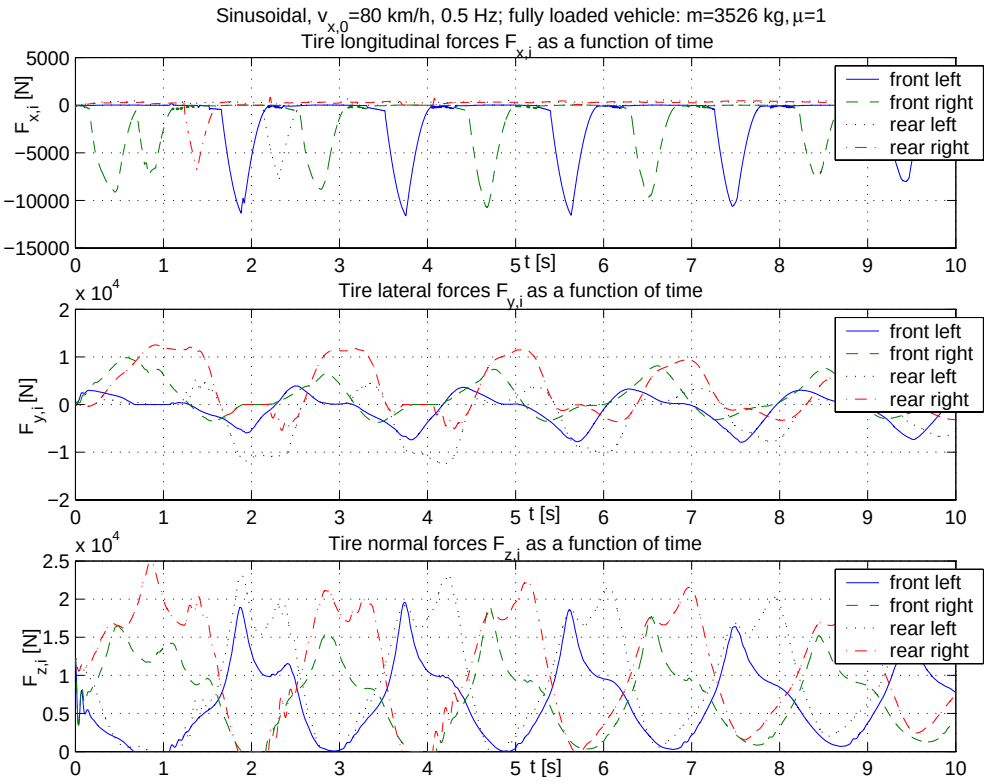

Figure 5.4: Force plots from simulation with a sinusoidal steering input ($135°$ and 0.5 Hz) for a fully loaded vehicle in 80 km/h using the Lyapunov controller that assumes full load.

Figure 5.4 shows the tire forces during the sinusoidal input. The uppermost plot illustrates the braking forces induced by the Lyapunov controller. It shows how the outer track is used for braking; first the front

wheel to stabilize the roll motion, and then the rear wheel to avoid skidding. After 2.5 s the slip motion does not need to be stabilized resulting in only front braking forces, which minimizes the risk of oversteering due to Figure 3.5. The mid-plot shows the variation of the lateral tire forces and the plot at the bottom illustrates the normal forces. Zero normal force indicates wheel liftoff, which occurs for both wheels on the inner track during the first 5 s. This is because the safety margins are minimized to show the limits of the controller. After wheel liftoff the vehicle is quickly stabilized resulting in full ground contact.

This shows that the Lyapunov controller stabilizes the roll and slip motion for extreme maneuvers and the vehicle follows the steering input well. The same results are obtained during simulations with the empty vehicle.

5.4.4 Steerability

This section will examine the steering properties of the vehicle using the Lyapunov controller.

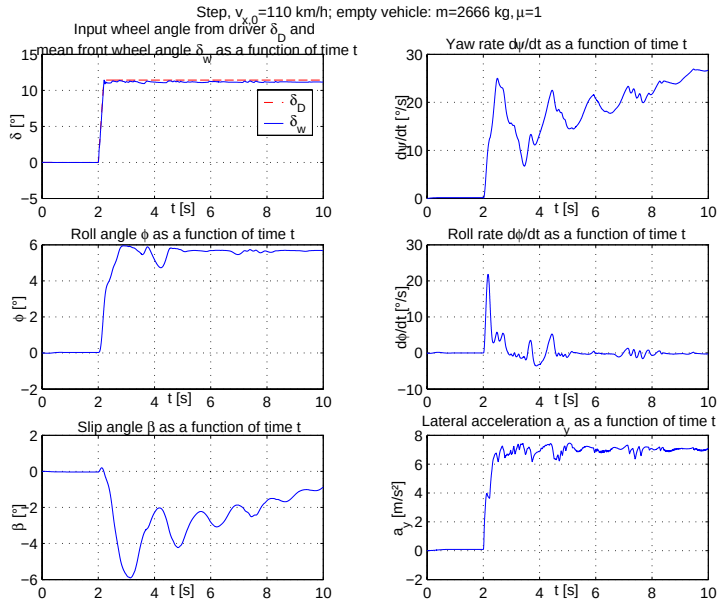

Figure 5.5: Plots from simulation of a step input (200°) for an empty vehicle in 110 km/h using the Lyapunov controller that assumes full load.

Figure 5.5 shows the plots from a simulation of a step input in 110 km/h

for the empty vehicle. The step on the steering wheel is $200°$ occurring at 2 s, with almost an infinite slope. The yaw rate $\dot{\psi}$ indicates how the vehicle is cornering, first it increases rapidly but decreases later due to the roll control, then it increases again and so on. The roll angle φ and the lateral acceleration a_y are stable around the values $5.7°$ and 7.1 m/s^2. The side slip β is just inside the limits and decreasing with time.

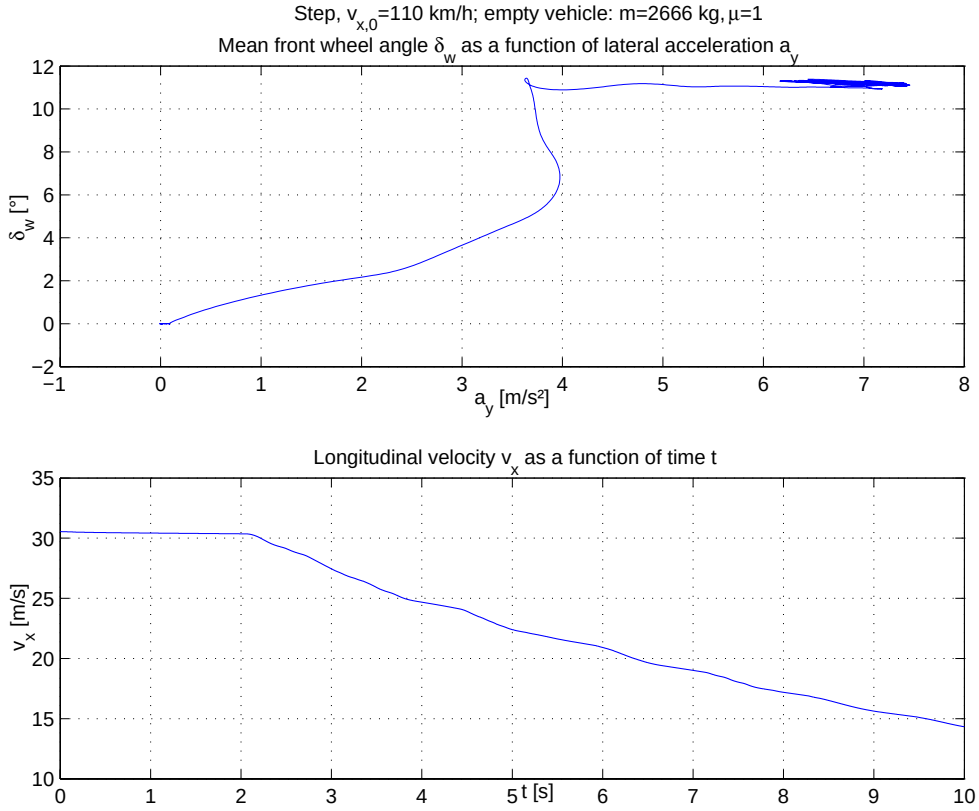

Figure 5.6: Steerability and velocity plots from simulation of a step input ($200°$) for an empty vehicle in 110 km/h using the Lyapunov controller that assumes full load.

The steerability and velocity of the vehicle is shown in Figure 5.6. Due to (3.7), (3.8), and (3.9) the steering properties of the vehicle can be determined through looking at the slope of the uppermost plot. Of course, during the initial phase when the wheel angle increases from $0°$ up to $11.4°$ the vehicle will understeer a bit. The interesting part is though during stationary motion, i.e. when the wheel angle has reached the stationary value

$11.4°$. Then the slope of the plot is approximately zero indicating neutral steering. The same results are obtained for the fully loaded vehicle.

5.4.5 Snow and Ice Driving

The simulations above and below are all performed on dry roads, i.e. the road-tire coefficient of friction $\mu = 1$. During snow conditions the coefficient $\mu = 0.4$.

The vehicle will almost never liftoff or roll during snow or ice driving, only skid. Therefore is the two-track model not satisfied, and the controller cannot be used. The only possibility that the vehicle will roll is if it starts to skid and then reaches an area of the road with higher friction and gets grip (tripped rollover). But this will be avoided using an ESP, which prevents the vehicle from skidding. If the vehicle even though starts to roll, a desired yaw rate (5.30) can still be calculated and processed in the ESP to stabilize the roll motion. See Chapter 7 for further discussion.

5.4.6 Comparison between the Lyapunov Controller and the LQ-controller

It also exists an old roll controller, namely a linear quadratic one (LQ), based on completely different theories. It is simulated in the same Simulink model as the Lyapunov controller. The only difference is that the S-function *sfdlyap.m* in the design above is exchanged for another S-function *sfdlqr.m*, which contains the LQ-controller.

The LQ-controller is simulated and compared to the new Lyapunov controller using plots and animations. The safety margins in both controllers are minimized to see the limits. When the vehicle model is run on a 2.8 GHz Pentium 4 processor the simulation with the Lyapunov controller is approximately 2.7 times faster than the simulation with the LQ-controller.

Figure 5.7 shows the comparison plots between the controllers for a chirp signal input to the empty vehicle. The amplitude of the signal is $135°$ and the frequency increases from 0.1 Hz to 2 Hz, covering the roll eigenfrequency of the vehicle. The yaw rate $\dot{\psi}$ is approximately equal for both controllers at the beginning, but the amplitude decreases faster for the LQ-controller at the end. The magnitude of the roll angle φ is a little bigger

for the Lyapunov controller in the first 3 s but still inside the limits, both controllers are equal after 3 s . The roll rate $\dot{\varphi}$ is approximately the same and the increasing amplitudes of both φ and $\dot{\varphi}$ is explained by the increasing frequency, but the amplitudes decrease again just around and after 10 s. The first 3 s indicates that the side slip is bigger for the Lyapunov controller, but all values are inside the allowed region.

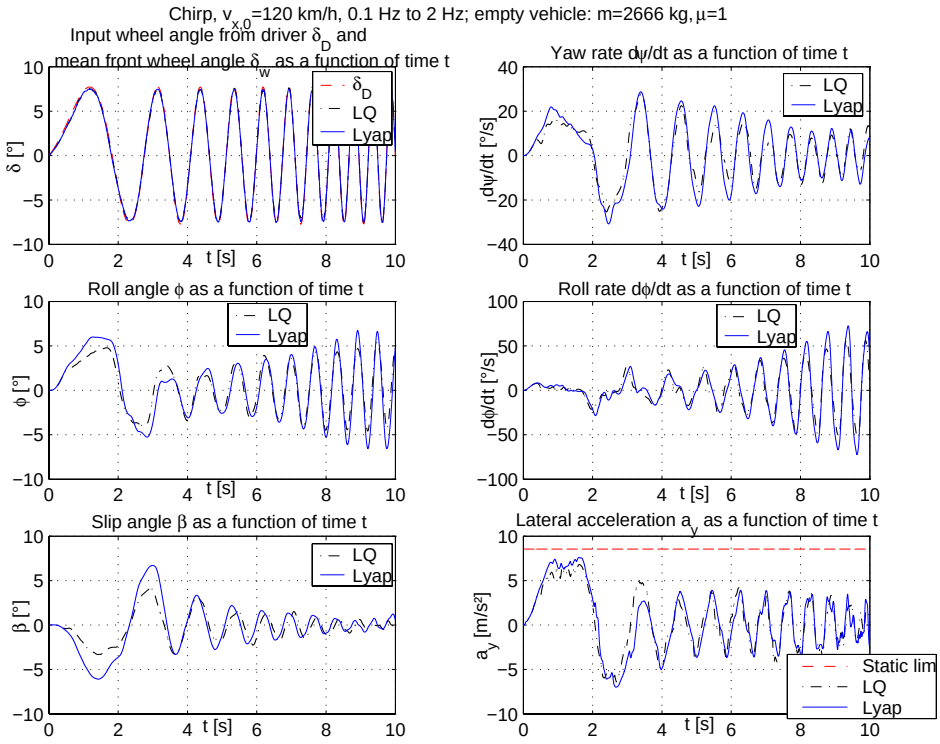

Figure 5.7: Plots from simulation with a chirp signal as input ($135°$ and 0.1 Hz $\rightarrow$ 2 Hz) for an empty vehicle in 120 km/h using the Lyapunov controller and the LQ-controller that assume full load.

The lowest plot to the right shows the lateral acceleration a_y of the different vehicles. The red curve illustrates the static limit of a_y, which is the highest lateral acceleration of the uncontrolled vehicle just before it rolls over, approximately 8 m/s^2. It can be seen that the curve corresponding to the Lyapunov controller is closer to this limit than the curve corresponding to the LQ-controller. This indicates that the Lyapunov controller is less conservative and allows the states to get closer to the limits than the LQ-controller, even though the safety margins are minimized for both controllers.

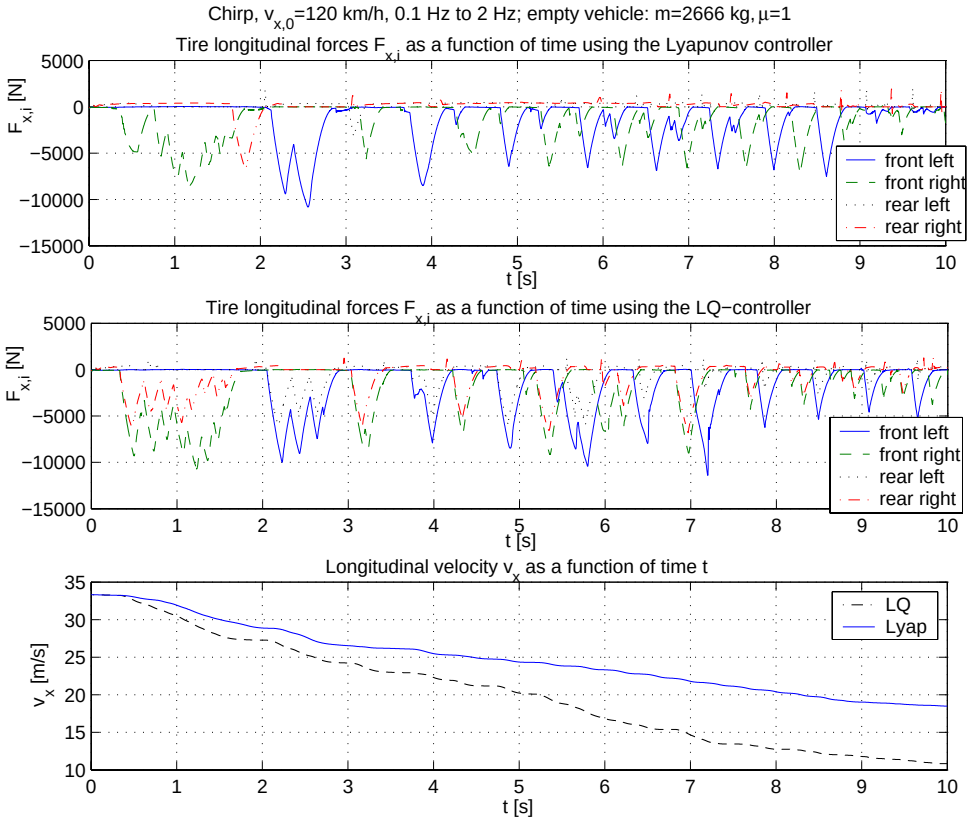

Figure 5.8: Force and velocity plots from simulation with a chirp signal as input (135° and 0.1 Hz $\rightarrow$ 2 Hz) for an empty vehicle in 120 km/h using the Lyapunov controller and the LQ-controller that assume full load.

The animation of the three vehicles (two with controllers and one without any control at all) shows that the uncontrolled vehicle rolls over in the first turn after 1.8 s. The controlled vehicles continue driving due to single-wheel braking that stabilizes the roll and slip motion. It can also be seen that the Lyapunov controlled vehicle overtakes the LQ-controlled, i.e. the Lyapunov one looses less energy due to less braking. This becomes obvious when analyzing the plots in Figure 5.8. The two uppermost plots show the braking forces from the Lyapunov controller respective the LQ-controller. As can be seen, the LQ-controller applies higher braking forces overall than the Lyapunov controller, especially on the rear outer wheel. The Lyapunov controller brakes only on the rear outer wheel during the first 3 s (the first two turns), when the slip motion needs to be stabilized, but the LQ-controller uses the rear outer brake during all 10 s. The lowest

plot showing the velocity v_x as a function of time t confirms that the LQ-controller brakes more since it looses more speed. This discussion shows once more that the Lyapunov controller is less conservative than the LQ-controller. Due to Figure 3.5 and the observation that the Lyapunov controller brakes less on the rear outer wheel than the LQ-controller, the risk of oversteering and un-stabilizing the vehicle is lower for the Lyapunov controller.

The last simulation is a fishhook, described in section 5.3. The amplitude of the signal is standardized to $162.5°$ on the steering wheel. Since it consists of a step to the left immediately followed by a longer step to the right it is very difficult to control the vehicle during this maneuver at high speeds.

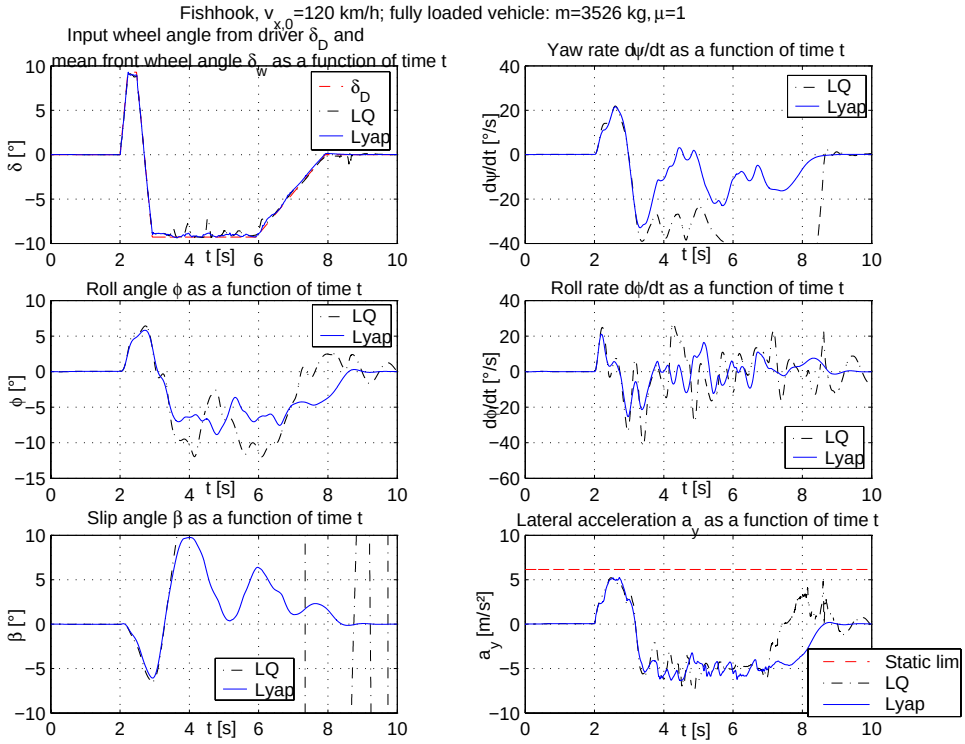

Figure 5.9: Plots from simulation of a fishhook ($162.5°$) for a fully loaded vehicle in 120 km/h using the Lyapunov controller and the LQ-controller that assume full load.

The animation shows rollover of the uncontrolled vehicle at 2.8 s, only 0.8 s after the start of the fishhook. The LQ-controlled vehicle starts to oversteer in the second turn at about 4.1 s, which results in skidding, spinning, and

leaving the desired path. This is also confirmed in the left lowermost plot in Figure 5.9 showing the slip angle β; it goes to infinity at about 4 s for the LQ-controller. The yaw rate $\dot{\psi}$ shows also the dangerous movement of the LQ-controlled vehicle. The Lyapunov controlled vehicle is the only one following the desired path all the way, see the yaw rate $\dot{\psi}$ in Figure 5.9. Both the roll angle φ and the side slip β is kept inside the limits. The right lowermost plot shows once again that the lateral acceleration a_y for the Lyapunov controlled vehicle is closest to the static limit (6.2 m/s^2); i.e. the Lyapunov controller is less conservative than the LQ-controller.

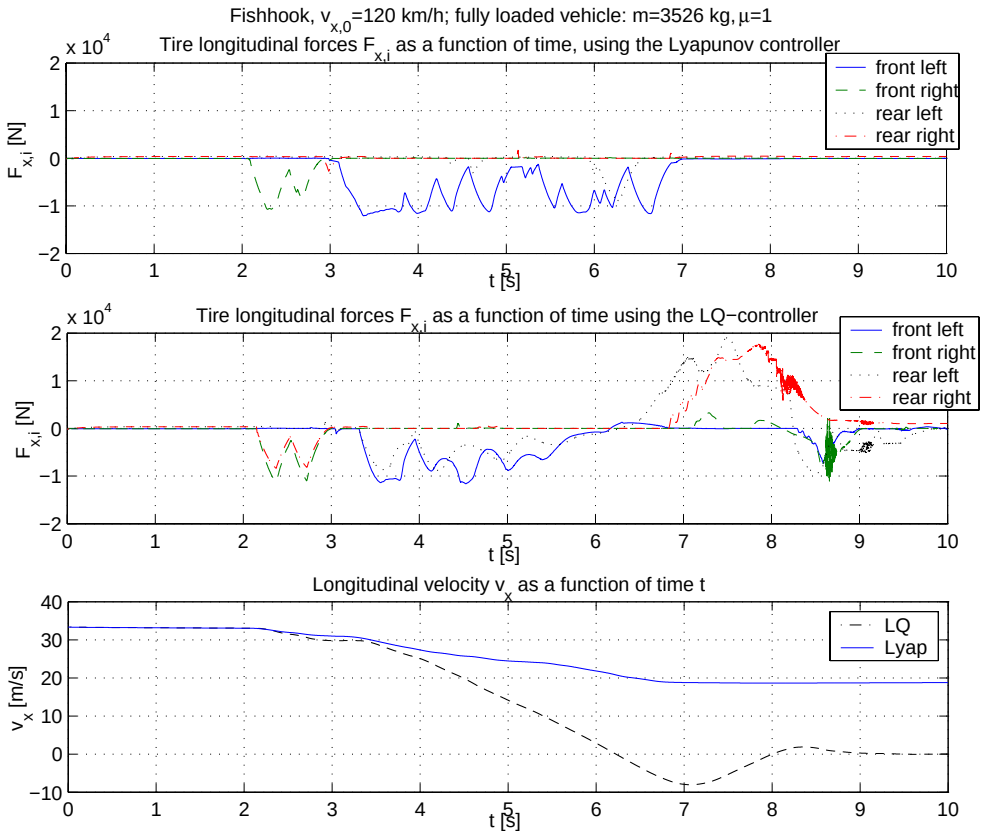

Figure 5.10: Force and velocity plots from simulation of a fishhook ($162.5°$) for a fully loaded vehicle in 120 km/h using the Lyapunov controller and the LQ-controller that assume full load.

The sudden oversteering behavior of the LQ-controlled vehicle can be explained through looking at the braking forces, see Figure 5.10. In the second turn (to the right) the LQ-controller puts on a braking force on the

rear left wheel, see the mid-plot in Figure 5.10. The braking force is big and lasts for more than 2 s. This probably results in oversteering of the vehicle according to Figure 3.5. The Lyapunov controlled vehicle uses the rear left brake much less (just to stabilize the slip motion), which avoids oversteering behavior. The lowermost plot shows the velocity v_x and once more the strange behavior of the LQ-controlled vehicle.

Chapter 6

Conclusions

This chapter sums up the most important results reached in this report. First it discusses rollover detection and then the control system.

6.1 Rollover Detection

Performed measurements show that it is possible to calculate each wheel load from measuring the spring deflections. This gives a way to detect wheel liftoff and possible rollover. But, since today's commercial vans do not have spring deflection sensors, another strategy is needed.

Assuming that the roll angle φ and the roll rate $\dot{\varphi}$ can be measured or estimated it is possible to calculate the total roll energy and the critical potential energy. Comparing these two quantities gives another way to detect rollover. This strategy is used in the development of the roll and slip controller.

6.2 Rollover Mitigation

Simulations show that the control system prevents rollover and skidding through stabilizing the roll and slip dynamics. The vehicle follows the desired steering input well. All this is proved for extreme maneuvers and at high speeds; even when one or two wheels have lost ground contact the

controller is able to stabilize the vehicle. Thus, the main objectives of this thesis are accomplished.

The controller is also robust; it works for both full and empty load conditions even though it assumes full load. No adaptive part to estimate the mass or center of gravity is needed, it would just slow down the controller.

The steering of the vehicle using the Lyapunov controller is mostly neutral, at some points it slightly understeers due to the braking on the outside wheels. There are no signs of oversteering.

The Lyapunov controller performs better than the already existing LQ-controller. It is much faster and less conservative since the lateral acceleration is closer to the limits and it brakes less; especially on the rear outer wheel, which reduces the risk of oversteering. The Lyapunov controller can be made more conservative easily through increasing the safety margins, which have been minimized during the simulations to show the limits of the controllers.

Chapter 7

Future Work

The tuning of the controller has to be optimized to find the best working set of safety margins and controller constants. It also needs to be simulated more for other maneuvers to see if the two-track model is enough. Maybe it has to be extended so it also covers the cases when the vehicle is on one and three wheels, but no indications of needing this has been seen so far.

The most important future work is to combine the robust Lyapunov controller with an observer that estimates for example the roll angle φ, which is unknown in the real vehicle. This will introduce uncertainties in the observed variables that can effect the performance of the controller.

Another important task is to integrate the Lyapunov controller with the ESP system, which will take care of skidding, under-, and oversteering. This results in avoiding tripped rollovers (see section 1.1), for example on snow or ice. An idea is to calculate the desired yaw rate (5.30) when rollover is detected and then process it in the ESP to stabilize the roll motion.

Lastly, the final control system must be tested in the real physical world, i.e. on a real test vehicle. This will of course introduce disturbances that can effect the controller negatively.

Bibliography

[1] Bergman, W. The Basic Nature of Vehicle Understeer-Oversteer. SAE-paper 957 B, 1965.

[2] CEmACS partners. Sixth Framework Programme, Priority 2, Information Society Technologies, May 2004. Information about the CEmACS project.

[3] Dahlberg, E. *Commercial Vehicle Stability - Focusing on Rollover*. PhD thesis, Royal Institute of Technology, Department of Vehicle Engineering, March 2001.

[4] Dahlgren, J. Robust nonlinear control design for a missile using backstepping. Master's thesis, Tekniska Högskolan i Linköping, 2003.

[5] Glad, T., Ljung, L. *Reglerteori. Flervariabla och olinjära metoder*. Studentlitteratur, 1994.

[6] Johansson, B. Untripped SUV Rollover Detection and Prevention. Master's thesis, Lund Institure of Technology, Department of Automatic Control, February 2004.

[7] Koibuchi, K., Yamamoto, M., Fukada, Y., Inagaki, S. Vehicle Stability Control in Limit Cornering by Active Brake. SAE-paper 960487, 1996.

[8] Küpper, S. Entwurf von Regelungsstrategien zur Kippstabilisierung von Kraftfahrzeugen. Master's thesis, DaimlerChrysler AG, 2000.

[9] Krstić, M., Kanellakopoulos, I., Kokotović, P. *Nonlinear and Adaptive Control Design*. John Wiley & Sons, Inc., 1995.

[10] MathWorks, Inc. *Matlab Online Documentation*. www.mathworks.com.

[11] Pacejka, H. B. *Tyre and Vehicle Dynamics*. Elsevier Butterworth Heinemann, 2002.

[12] Popp, K., Schiehlen, W. *Fahrzeugdynamik*. B. G. Teubner, 1993.

[13] LaTeX project team. *LaTeX homepage*. www.latex-project.org.

[14] Schindler, E. Vehicle Dynamics.

[15] Sepulchre, R., Janković, M., Kokotović, P. V. *Constructive Nonlinear Control*. Springer, August 1996.

[16] Slotine, J-J. E., Li W. *Applied Nonlinear Control*. Prentice Hall International Inc., 1991.

[17] Wong, J. Y. *Theory of Ground Vehicles*. John Wiley & Sons, Inc., 2001.

Appendix A

Vehicle Parameters

Parameter	Explanation [unit]	Value
m	mass [kg]	2666
J_{xx}	moment of inertia about the x-axis [kgm^2]	1800
J_{yy}	moment of inertia about the y-axis [kgm^2]	8400
J_{zz}	moment of inertia about the z-axis [kgm^2]	8830
l_F	horizontal distance from the front axle to the CoG [m]	1.58
l_R	horizontal distance from the rear axle to the CoG [m]	1.97
h_{CoG}	height from the ground to the CoG [m]	0.850
s_F	front track width [m]	1.652
s_R	rear track width [m]	1.652
c_φ	roll stiffness, mean of both axles [Nm/rad]	221057
d_φ	roll damping, mean of both axles [Nm/rad]	11216

Table A.1: Vehicle parameters for the empty commercial van.

Parameter	Explanation [unit]	Value
m	mass [kg]	3526
J_{xx}	moment of inertia about the x-axis [kgm^2]	2275
J_{yy}	moment of inertia about the y-axis [kgm^2]	13400
J_{zz}	moment of inertia about the z-axis [kgm^2]	13990
l_F	horizontal distance from the front axle to the CoG [m]	2.2114
l_R	horizontal distance from the rear axle to the CoG [m]	1.3386
h_{CoG}	height from the ground to the CoG [m]	1.135
s_F	front track width [m]	1.652
s_R	rear track width [m]	1.652
c_φ	roll stiffness, mean of both axles [Nm/rad]	221057
d_φ	roll damping, mean of both axles [Nm/rad]	11216

Table A.2: Vehicle parameters for the fully loaded commercial van.